

**Investigation of Dosimetric Properties and Kinetic  
Parameters of Cu and Pr doped Sr<sub>2</sub>P<sub>2</sub>O<sub>7</sub>**

**M.Sc Thesis  
in  
Engineering of Physics  
University of Gaziantep**

**Supervisor  
Prof.Dr. A.Necmeddin YAZICI**

**by  
Mustafa ASLAN  
February 2012**

©2012 [MUSTAFA ASLAN].


REPUBLIC OF TURKEY  
UNIVERSITY OF GAZİANTEP  
GRADUATE SCHOOL OF NATURAL & APPLIED SCIENCES  
DEPARMENT OF ENGINEERING PHYSICS

Name of thesis : Investigation of Dosimetric Properties and Kinetic  
Parameters of Cu and Pr doped  $Sr_2P_2O_7$


Name & Surname of Student: Mustafa ASLAN

Exam date :13.02.2012

Approval of the Graduate School of Natural Science and Applied Science

  
Prof. Dr. Ramazan Koç  
Director

I certify that this thesis satisfies all the requirements as a thesis for degree of Master  
of science.

  
Prof. Dr. A. Necmeddin Yazıcı  
Head of Department

This is to certify that we have read this thesis and that in our consensus/majority  
opinion it is fully adequate, in scope and quality, as a thesis for the degree of Master  
of Science.


  
Prof. Dr. A. Necmeddin YAZICI  
Supervisor

Examining Committee Members  
Prof. Dr. A. Necmeddin YAZICI  
Prof. Dr. Zihni ÖZTÜRK  
Assoc. Prof. Dr. Hüseyin BOZKURT  
Assoc. Prof. Dr. Okan ÖZER  
Asist. Prof. Dr. Hüseyin TOKTAMIŞ

Signature  


**I hereby declare that all information in this document has been obtained and presented in accordance with academic rules and ethical conduct. I also declare that, as required by these rules and conduct, I have fully cited and referenced all material and results that are not original to this work.**

Mustafa ASLAN

A handwritten signature in black ink, appearing to read "J. M. Aslan" or "Mustafa Aslan", written in a cursive style.

## ABSTRACT

### INVESTIGATION of DOSIMETRIC PROPERTIES and KINETIC PARAMETERS of Cu and Pr DOPED $\text{Sr}_2\text{P}_2\text{O}_7$

ASLAN, MUSTAFA

M.SC. in Engineering of Physics

Supervisor: Prof. Dr. Necmeddin YAZICI

February 2012

70 pages

In this study; the TL dosimetric properties and kinetic parameters of Cu and Pr-doped  $\text{Sr}_2\text{P}_2\text{O}_7$  were investigated. The investigations on pure  $\text{Sr}_2\text{P}_2\text{O}_7$  were indicated that it has one glow peak around 100 °C. On the other hand, it was observed that the Cu and Pr doped  $\text{Sr}_2\text{P}_2\text{O}_7$  has two glow peaks around 100 °C and 200 °C. The detail dosimetric studies of glow peak around 200 °C were shown that this material can be one of the promising TLD material for dosimetric applications, i.e., personal dosimeter. The kinetic parameters of  $\text{Sr}_2\text{P}_2\text{O}_7:\text{Cu,Pr}$  were analyzed by different methods such as additive dose (AD),  $T_M - T_S$ , repeated initial rise (RIR), peak shape(PS) and computer glow curve deconvolution (CGCD). The additive dose technique was indicated that the kinetic orders of glow peaks of this sample were described with first-order kinetics. But the other methods were indicated that they have general-order kinetics. The results were shown that there is no good agreement and consensus between the kinetic parameters by various techniques due the variation in the emission spectrum of this sample with temperature, self-absorption and thermal quenching.

**Keywords:** thermoluminescence, dosimetry, kinetic parameter,  $\text{Sr}_2\text{P}_2\text{O}_7:\text{Cu,Pr}$

## **ACKNOWLEDGEMENT**

I would like to thank my supervisor Prof. Dr. A. Necmeddin Yazıcı because of his helps and advice during this study. Secondly I wish to thank also Assist Prof. Dr. Hüseyin Toktamış because of helping in experimental procedure. Thirdly I wish to thank also Semih Seyyidođlu and Ayşen Yılmaz who are from Middle East Technical University (ODTÜ) for preparing the sample. Finally I would like to thank other personnel at the department of Engineering Physics for their kind and friendships.

## TABLE OF CONTENTS

CONTENTS	page
ABSTRACT .....	iv
ÖZ.....	v
ACKNOWLEDGEMENT .....	vi
CONTENTS .....	vii
LIST OF FIGURES .....	viii
CHAPTER 1: Introduction .....	1
CHAPTER 2: THEORY OF THERMOLUMINESCENCE .....	4
2.1. Basic Concepts of Thermoluminescence .....	4
2.2. Applications of TL Dosimeters .....	7
2.3. The General Characteristics of TL Dosimeters.....	8
2.4. Types of Luminescence .....	9
2.5. Electronic Transitions within the Band Gap of Insulators and Semiconductors .....	10
2.6. The One Trap–One Recombination (OTOR) Centre Model.....	12
2.7. Trap-Filling Process .....	13
2.8. Trap-Emptying Process .....	14
2.9. First-order kinetics .....	17
2.10. Second-order kinetics .....	20
2.11. General-order kinetics .....	22
2.12. Trapping Parameters Determination Methods .....	23
2.12.1. CGCD Method .....	24
2.12.2. Initial Rise Method .....	26
2.12.3 Heating Rate Method .....	27
2.12.4. Peak Shape Methods .....	28
CHAPTER 3: EXPERIMENTAL PROCEDURE .....	30
3.1. Synthesis of Samples .....	30
3.2. Equipments .....	33
3.2.1 Annealing Ovens and General Heat Treatment .....	33
3.2.2 Radiation Source and Irradiation Procedure .....	33
3.2.3 TL Analyzer and TL Measurements .....	33
3.3 Experimental Procedure .....	34
CHAPTER :4 EXPERIMENTAL RESULTS and DISCUSSIONS .....	36
4.1. Effect of Doping Concentration of Cu and Pr on the Glow Peaks of Sr <sub>2</sub> P <sub>2</sub> O <sub>7</sub> .....	36
4.2. Annealing Procedure of Sr <sub>2</sub> P <sub>2</sub> O <sub>7</sub> :Cu,Pr .....	37
4.3. The glow curve analysis of Sr <sub>2</sub> P <sub>2</sub> O <sub>7</sub> :Cu,Pr .....	39
4.4. Determination of Number and Position of Glow Peaks by $T_m(E_a)-T_{stop}$ Method .....	44
4.5. Glow Curves Analysis by CGCD Method .....	52
4.6. The Influence of Heating Rate .....	55
4.7. Fading Studies at Room Temperature .....	57
4.8. Dose Response .....	60
CHAPTER 5: CONCLUSION .....	62
References .....	64

## LIST OF FIGURES

	page
Figure 2.1: Phenomena of thermal excitation of luminescence .....	4
Figure 2.2: Simple diagram of a TL reader system with heater plate, photomultiplier detector and readout electronics .....	5
Figure 2.3: An analyzed glow curve of Ce-doped MgB <sub>4</sub> O <sub>7</sub> measured after 36 Gy irradiation at room temperature at a heating rate of 1°Cs <sup>-1</sup> [42] .....	6
Figure 2.4: Common electronic transitions in crystalline solids: (1) ionization; (2) electron trapping; (3) electron release; (4) direct recombination; (5) indirect recombination. (ET: Electron Trap; RC: Recombination Centers) [49] .....	11
Figure 2.5: Simple band model for TL emission. Allowed transitions: (1) thermal release, (2) migration in the conduction band, (3) radiative recombination [2] .....	13
Figure 2.6: Properties of the Randall–Wilkins first-order TL equation, showing: (a) variation with $n_0$ , the concentration of trapped charge carriers after irradiation; (b) the variation with $E$ , the activation energy; (c) the variation with $s$ , the escape frequency; (d) the variation with $\beta$ , the heating rate. Parameter values: $n_0=1\text{ m}^{-3}$ ; $E=1\text{ eV}$ ; $s=1\times 10^{12}\text{ s}^{-1}$ , $\beta=1\text{ K/s}$ of which one parameter is varied while the others are kept constant [58] .....	19
Figure 2.7: Properties of the Garlick–Gibson second-order TL equation, showing: (a) variation with $n_0$ , the concentration of trapped charge carriers after irradiation; (b) the variation with $E$ , the activation energy; (c) the variation with $s/N$ ; (d) the variation with $\beta$ , the heating rate. Parameter values: $n_0=1\text{ m}^{-3}$ ; $E=1\text{ eV}$ ; $s/N=1\times 10^{12}\text{ s}^{-1}\text{ m}^3$ , $\beta=1\text{ K/s}$ of which one parameter is varied while the others are kept constant [64] .....	22
Figure 2.8: Comparison of first-order ( $b=1$ ), second-order ( $b=2$ ) and intermediate-order ( $b=1.3$ and $1.6$ ) TL peaks, with $E=1\text{ eV}$ , $s=1\times 10^{12}\text{ s}^{-1}$ , $n_0=N=1\text{ m}^{-3}$ and $\beta=1\text{ K/s}$ [49].....	23
Figure 2.9: The characteristics points on a TL glow-peak, which define the peak-shape parameters. [77] .....	28
Figure 2.10: Geometrical factor ( $\mu_g$ ) as a function of the given order. [49] .....	29
Figure 3.1: X-ray powder diffraction pattern of orthorhombic Sr <sub>2</sub> P <sub>2</sub> O <sub>7</sub> [1].....	31



Figure 3.2: The powder X-ray diffraction patterns of 5% CuO and (a) 3%, 2%, 1%, and 0.5% Pr <sub>6</sub> O <sub>11</sub> doped Sr <sub>2</sub> P <sub>2</sub> O <sub>7</sub> and (b) 15%, 10%, 5%, and 4% Pr <sub>6</sub> O <sub>11</sub> doped Sr <sub>2</sub> P <sub>2</sub> O <sub>7</sub> [1] .....	32
Figure 3.3: Experimental equipments (a) <sup>90</sup> Sr- <sup>90</sup> Y β-source (b) 9010 Optical Dating System (c) Harshaw TLD System 3500.....	34
Figure 4.1: The thermoluminescence glow curves of %5 Cu and various Pr doped Sr <sub>2</sub> P <sub>2</sub> O <sub>7</sub> samples [1] .....	36
Figure 4.2: Reproducibility of deconvoluted areas of glow peaks: (a) peak 1 and (b) peak 2 of Sr <sub>2</sub> P <sub>2</sub> O <sub>7</sub> :Cu,Pr through ten repeated cycles of irradiation-readout annealing.....	39
Figure 4.3: The glow curve of Sr <sub>2</sub> P <sub>2</sub> O <sub>7</sub> :Cu,Pr measured after various radiation dose levels ( $\beta=1\text{ }^{\circ}\text{C s}^{-1}$ ).....	41
Figure 4.4: The peak temperatures $T_m$ of glow peaks of Sr <sub>2</sub> P <sub>2</sub> O <sub>7</sub> :Cu,Pr as a function of exposed dose level.....	42
Figure 4.5: The peak temperature $T_m$ , low half-maximum temperature $T_1$ and high half-maximum temperature $T_2$ of dosimetric glow peak of Sr <sub>2</sub> P <sub>2</sub> O <sub>7</sub> :Cu,Pr as a function of exposed dose level.....	42
Figure 4.6: The geometric factor $\mu_g$ of dosimetric glow peak of Sr <sub>2</sub> P <sub>2</sub> O <sub>7</sub> :Cu,Pr as a function of exposed dose level.....	43
Figure 4.7: The activation energy $E_a$ of the dosimetric glow peak of Sr <sub>2</sub> P <sub>2</sub> O <sub>7</sub> :Cu, Pr determined by PS method as a function of exposed dose levels ( $\beta = 1^{\circ}\text{C s}^{-1}$ )... 44	44
Figure 4.8: Some of the selected glow curves of Sr <sub>2</sub> P <sub>2</sub> O <sub>7</sub> :Cu,Pr after different $T_{\text{stop}}$ temperatures between 59 °C and 134 °C at a linear heating rate $\beta = 1\text{ }^{\circ}\text{C s}^{-1}$ . The exposed dose levels are always adjusted to $\approx 12\text{ Gy}$ .....	45
Figure 4.9: Some of the selected glow curves of Sr <sub>2</sub> P <sub>2</sub> O <sub>7</sub> :Cu,Pr after different $T_{\text{stop}}$ temperatures between 139 °C and 214 °C at a linear heating rate $\beta = 1\text{ }^{\circ}\text{C s}^{-1}$ . The exposed dose levels are always adjusted to $\approx 12\text{ Gy}$ .....	46
Figure 4.10: $I_m-T_{\text{stop}}$ plot for the thermoluminescent glow peaks of Sr <sub>2</sub> P <sub>2</sub> O <sub>7</sub> :Cu,Pr.....	47
Figure 4.11: $T_m-T_{\text{stop}}$ plot for the thermoluminescent glow peaks of Sr <sub>2</sub> P <sub>2</sub> O <sub>7</sub> :Cu,Pr.....	48
Figure 4.12: (a) The geometric factor $\mu_g$ , $T_2-T_1$ and $T_2-T_m$ of low temperature glow peak of Sr <sub>2</sub> P <sub>2</sub> O <sub>7</sub> :Cu,Pr as a result of $T_{\text{stop}}$ determined from the $T_m-T_{\text{stop}}$ procedure. Lines are fits to guide the eye. (b) The activation energy ( $E_a$ ) resulting from the PS method after the $T_m-T_{\text{stop}}$ procedure .....	49

Figure 4.13: (a) The geometric factor $\mu_g$ , $T_2-T_1$ and $T_2-T_m$ of high temperature dosimetric glow peak of $\text{Sr}_2\text{P}_2\text{O}_7:\text{Cu,Pr}$ as a result of $T_{\text{stop}}$ determined from the $T_m-T_{\text{stop}}$ procedure. Lines are fits to guide the eye. (b) The activation energy ( $E_a$ ) resulting from the PS method after the $T_m-T_{\text{stop}}$ procedure.....	50
Figure 4.14: The activation energy ( $E_a$ ) resulting from the RIR method after $T_m-T_{\text{stop}}$ procedure.....	52
Figure 4.15: Some of the CGCD analyzed glow curves after different $T_m-T_{\text{stop}}$ experiments ( $D \approx 12$ Gy). In all figures, open circles, solid lines and dotted lines represent the experimental points, global fitting and fitted individual peaks, respectively ( $\beta = 1^\circ\text{C s}^{-1}$ ).....	54
Figure 4.16: The kinetic parameters ( $E_a$ , s, b) and peak intensities ( $I_m$ ) of glow peaks of $\text{Sr}_2\text{P}_2\text{O}_7:\text{Cu,Pr}$ resulting from the CGCD method after $T_m-T_{\text{stop}}$ procedure.....	55
Figure 4.17: (a) Some of the selected glow curves of $\text{Sr}_2\text{P}_2\text{O}_7:\text{Cu,Pr}$ measured at various heating rates from $1^\circ\text{C s}^{-1}$ to $30^\circ\text{C s}^{-1}$ . All the glow curves were measured after $\beta$ -irradiation to a dose level of $\approx 12$ Gy (b) The peak temperatures ( $T_m$ ) and thermoluminescence response ( $I_m$ ) of glow peaks of $\text{Sr}_2\text{P}_2\text{O}_7:\text{Cu,Pr}$ as a function of heating rate [1].....	56
Figure 4.18: Fading evaluation of the deconvoluted peaks of $\text{Sr}_2\text{P}_2\text{O}_7:\text{Cu,Pr}$ at room temperature in the dark room. ....	58
Figure 4.19: Variable heating rate plots of $\ln(T_m^2/\beta)$ againsts ( $1/T_m$ ) of glow peaks. (a) Peak 1, (b) peak 2.....	59
Figure 4.20: The TL dose response curve of glow peaks of $\text{Sr}_2\text{P}_2\text{O}_7:\text{Cu,Pr}$ sample determined by the peak area of glow peaks.....	61

# CHAPTER 1

## INTRODUCTION

The TL dosimetries have been successfully used for radiation monitoring of personnel working around sources of ionizing radiations in the last forty years [1]. Recently, the use of TL dosimeter is especially increasing in radiation therapy [2]. Relative to the radiation therapy area, the studies on dosimetries continue on different areas [3]. Up to now, many kinds of materials, for instance, phosphate, sulfate, fluoride, borate, and oxide have been researched for finding an excellent thermoluminescence material [4]. There are many kinds of commercial thermoluminescence materials, but a few of them can be used in practice. Therefore, in order to discover a commercial dosimeter, the researches continue on the materials for TL dosimetry that have effective storage property. In this study, the TL properties of Cu and Pr doped  $\text{Sr}_2\text{P}_2\text{O}_7$  were investigated.

Recently, different pyrophosphates like pure and doped have an important role in technology because of their features of luminescent, semiconductor, dielectric, catalytic, fluorescent, magnetic, and ion-exchange. Due to these features, there are many research going on about the synthesis of pyrophosphates [5–14]. For example, the semiconductive features of Ti and Zr pyrophosphate catalysts have been worked by Marcu et al [15]. The effect of tetravalent metals on the dielectric properties of  $\text{ZrP}_2\text{O}_7$  and  $\text{Ti}_2\text{O}_7$  was determined by Kim et al (1999) [16] and Amezawa looked at high temperature protonic conduction in  $\text{Sr}_2\text{P}_2\text{O}_7$ - $\text{LaPO}_4$  systems [17].

There are many investigations on the luminescent applications of pyrophosphates. Doat et al. [18] described allotropic forms and photoluminescent properties of europium-doped calcium pyrophosphates while Schipper et al. [19] examined the luminescence of hafnium pyrophosphate, which emit in the UV spectral range. In recent years, the crystal structure and luminescence spectra of a new potassium erbium pyrophosphate dihydrate  $\text{ErKP}_2\text{O}_7 \cdot 2\text{H}_2\text{O}$  were published by

Assaaoudi et.al. [20]. Ce-doped luminescence of the first lutetium diphosphate  $\text{NH}_4\text{LuP}_2\text{O}_7$  was shown by Li et al. [21].

In general, the metals of group I elements are rapidly -diffusing impurities in many compounds [22]. Therefore, the Cu-impurity diffuses through the  $\text{Sr}_2\text{P}_2\text{O}_7$  lattice without any problem [23] and it is penetrate into the  $\text{Sr}_2\text{P}_2\text{O}_7$  lattice as a  $\text{Cu}^{2+}$ -ion in substitutional or interstitial sites. In the first case, it acts as an acceptor, and in the later, it acts as a donor. The  $\text{Cu}^{2+}$ -ions can also be converted to  $\text{Cu}^+$ -ion by capturing a free electron during the irradiation of materials by high energetically particles. In general, the presence of copper ions ( $\text{Cu}^+$ ,  $\text{Cu}^{2+}$ ) in the  $\text{Sr}_2\text{P}_2\text{O}_7$  lattice creates different energy levels within the band gap. They can act as electron and hole traps which are responsible with the glow peaks in Cu-doped  $\text{Sr}_2\text{P}_2\text{O}_7$  compounds.

The rare-earth dopants are known as very effective activators in host materials to create excellent TL features in TL materials. Because the attractive feature of lanthanides is their highly effective narrow band *f-f* photoluminescence coming from trivalent lanthanide ions independent from its environment: inorganic glass, sol-gel materials, polymers and in liquid crystals emit luminescence. Luminescences of lanthanide are complex because the transition occurs in *f* levels prevented by the influence of outer forces by filled *5s* and *5p* shells [24].

The TL features of strontium pyrophosphates have been studied by various scientific investigation groups among pyrophosphates. Because, the rare earth activated inorganic phosphors have broadly used in a many applications, as production of lamp, radiation dosimetry, TL dosimetry, imaging by X-ray, and color monitors [25]. Especially; the luminescent features of europium-ion activated phosphors for its applications in these application areas. The luminescence of  $\text{Eu}^{2+}$ -ions depend on the lattice because of crystal-field effects and changes from blue to red.  $\text{Eu}^{2+}$  activated strontium pyrophosphate emits luminescence at 420 nm without role of UV light, that is why it can be used in treating infants safely and also can be used in lamps for the photo-therapy,  $\text{Eu}^{2+}$  and  $\text{Mn}^{2+}$  co-doped  $\text{Sr}_2\text{P}_2\text{O}_7$  has been recommended to obtain white light emission from UV-LED devices [26].

The structural analyses of pyrophosphate compounds detail studied in the literature [27-38]. Different ways can be used in order to synthesize metal pyrophosphate compounds. Scientists have researched the structure of

pyrophosphate compounds by performing the help of different methods [9-14]. However, there is no research on the metal and metal-doped pyrophosphate compounds.

TL properties of different materials have been studied for a long time. But, there is relatively less amount of research upon TL of pyrophosphates in the literature survey. Natarajan et. al. [25] have worked on Eu-ion doped strontium pyrophosphate to study its TSL, PL and EPR. Miyoshi and Yoshino [39] have prepared calcium pyrophosphate ( $\text{Ca}_2\text{P}_2\text{O}_7$ ) which exhibited TL with X-ray and  $\gamma$ -ray irradiation. Kundua and et al. [40] have synthesized sodium pyrophosphate doped with  $\text{Dy}_2\text{O}_3$  purpose to develop a TL detector. However, Seyyidođlu at al.[1, 41] were demonstrated that strontium pyrophosphate had promising results for its TL property and it gave needed thermoluminescence intensity for radiation dosimetry when doped by some rare earth elements. It was found that the TL glow curves of pure  $\text{Sr}_2\text{P}_2\text{O}_7$  samples have a high intensive glow peak around 100 °C. Pr, Nd, Ho, and Er along Cu-doped samples resulted with very intensive and sharp glow peaks in thermoluminescence glow curves near 200 °C, the TL glow curve measurements have especially demonstrated that Pr and Cu-doped  $\text{Sr}_2\text{P}_2\text{O}_7$  exhibit very significant thermoluminescence glow peaks, suggesting these could be promising dosimetric materials. Bearing this in mind, some TL dosimetric properties and TL kinetic parameters of  $\text{Sr}_2\text{P}_2\text{O}_7:\text{Cu},\text{Pr}$  compounds were investigated in detail in this thesis, confirming they are promising for this application.

## CHAPTER 2

### THEORY OF THERMOLUMINESCENCE

#### 2.1. Basic Concepts of Thermoluminescence

After exposure to ionizing radiations, free electrons and holes are produced in insulating crystal and many of them are trapped in the crystal defects. When the crystal is heated, the trapped electrons are removed from traps and pass the conduction band (CB) and then they recombine with holes at the recombination centers. This recombination yields emission of light for different wavelengths. This process is called as thermoluminescence (TL). The curves plotted versus temperature and intensity of light is called TL glow curves. The thermoluminescent substances absorb some amount of the energy, which is stored for the duration of exposure to ionizing radiation and then if the substance is heated, the stored energy is changed to the form of visible light as shown in the Figure 2.1.

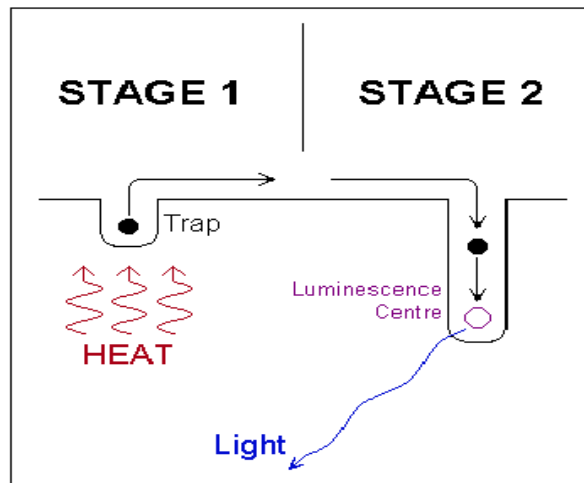


Figure 2.1: Phenomena of thermal excitation of luminescence.

A simple set up diagram to measure the TL intensity is demonstrated in Figure 2.2 and a typical TL glow curve obtained from Ce-doped  $\text{MgB}_4\text{O}_7$  sample is shown in Figure 2.3. The TL peaks are shaped by the record of emission light by intensity as function of temperature. A TL glow curve is similar a smooth continuum

but it is composed of a many overlapping peaks obtained by release of electrons from traps of different stabilities when they are heated.

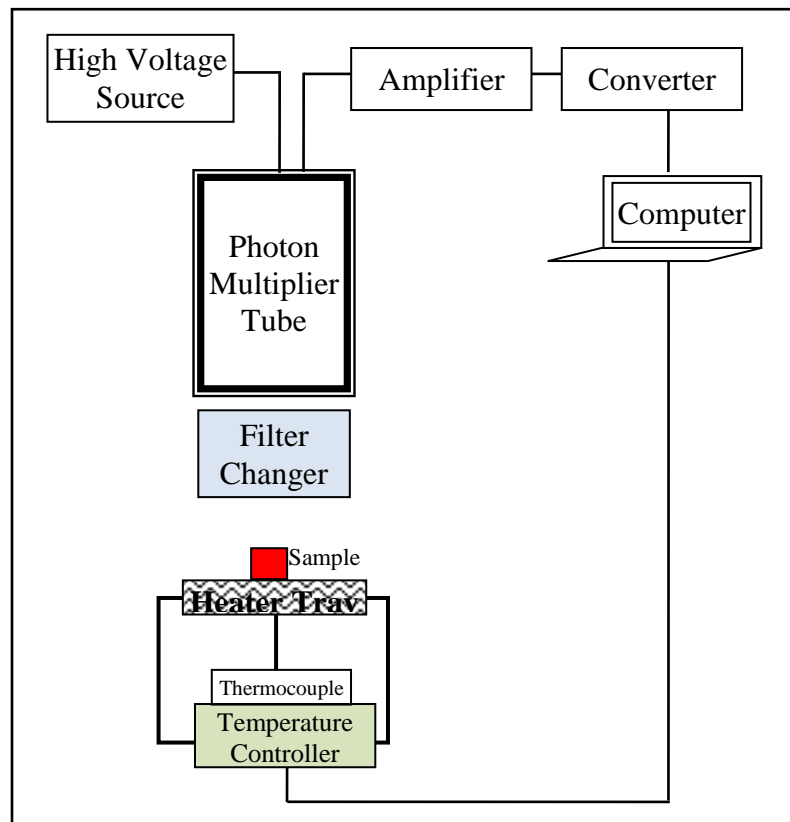


Figure 2.2: Simple diagram of a TL reader system with heater plate, photomultiplier detector and readout electronics.

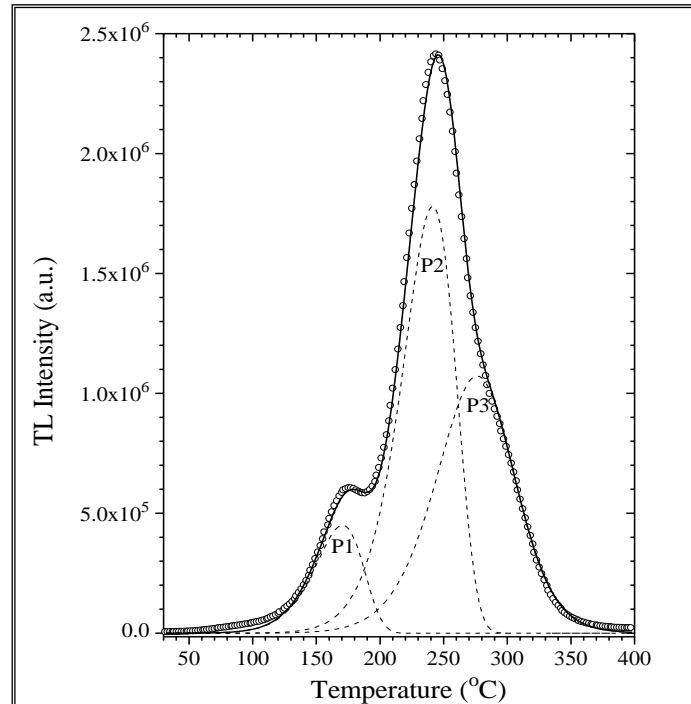


Figure 2.3: An analyzed glow curve of Ce-doped  $\text{MgB}_4\text{O}_7$  measured after 36 Gy irradiation at room temperature at a heating rate of  $1^\circ\text{C s}^{-1}$  [42].

Under favorable conditions, the TL light intensity is depend on the amount of absorbed dose. Because of this, using an appropriate calibration of TL dosimetry, one can evaluate the applied dose in the given radiation field. The emission of light intensity at its peak maximum and the area of that peak are proportional with absorbed dose. In regular dosimetric applications, one can choose an appropriate material with reproducible results in repeated measurements, linear dose dependence for the kind of radiation in question as well as dose-rate independence and longtime stability [43]. In addition, the certain information about kinetic parameters for the trapping process, frequency factor  $s$ , trap depth and kinetic order can be found from the position and shape of the glow curve. The TL mechanism governing the trapping and thermally release of electrons are given in the textbook of McKeever [2].

Three essential ingredients are required to the production of TL. Firstly, the samples have to be a band gap. Metals do not show luminescent properties because they don't have band gap. Secondly, the materials must have absorbed energy throughout exposure to ionizing radiation. Thirdly, the luminescence emission is should be start by heating the material [44]. TL material cannot emit light again by simply cooling the sample and reheating it another time. It should first be re-exposed



to ionizing radiation before it emits light again. The storage capacity of TL materials makes them suitable for dosimetric studies.

The TL process has been studied for a many years and nowadays there are many application of TL. The first application of it is in dosimetric purpose which was done by Daniel et al [45]. Then, many investigations have been carried out to understand TL phenomena and develop the TL characteristics of newly improved TLDs. Nowadays; the TLD is a well-established dosimetric method of the applications of personnel, environmental and clinical dosimetry [46].

The TL emission properties of materials, its sensitivity and absorbed energy can be affected by kinetic parameters. Thereupon, a good dosimetric work have to include base on a good information of kinetic parameters of materials. For instance, the exact information about lifetime of trapped electrons and fading rate are obtained from the trapping parameters of defects and they are obtained by using TL glow curves with different methods [2]. If any glow peak is separated from the other glow peaks, the trapping parameters can be obtained by classical methods such as heating rates (HR), initial rise (IR), and peak shape (PS). However, in most materials, the glow curve includes several overlapping peaks. If there are many glow peaks in the glow curve, there are two ways to obtain exact parameters: the first one is to isolate each individual TL peak from the others using partial thermal annealing treatment and the other way is to using of glow curve analysis using by computer deconvolution [47].

The essential propose of this study is to research the dosimetric features and kinetic parameters of  $\text{Sr}_2\text{P}_2\text{O}_7:\text{Cu},\text{Pr}$ . To do this, the TL dosimetric properties of glow peaks after beta-irradiation between the dose level  $D = 0.04\text{Gy}$  and  $D = 4.6 \text{ kGy}$  and kinetic parameters of this sample were studied by the following methods:  $T_m(E_a)$ – $T_{\text{stop}}$ , repeated initial rise (RIR), peak shape (PS), additive dose (AD) and (CGCD) [47–50]. The dose response can be examined by peak height and peak area methods.

## **2.2. Applications of TL Dosimeters**

The thermoluminescence applications have many benefits in human life. Some of applications of TL dosimetries are:

1. In radiation displaying: a) Personnel displaying, b) Environmental displaying

2. In experimental dosimetry: a) Natural background works, b) source calibrations, c) high energy physics works
3. In nuclear medicine: a) Therapy displaying, b) measurement of doses in sensitive organs and areas, c) Internal emitter dosimetry, d) phantom dosimetry
4. In geology: calculating the age of rocks [51].

### **2.3. The General Characteristics of TL Dosimeters**

A dosimetry system along with its reader is named as a dosimetry system. It evaluates either directly or indirectly the quantities of exposure, kerma, absorbed dose, equivalent dose, or their time derivatives (rates), or related quantities of ionizing radiation. Radiation dosimeters must have some characteristics according to their application areas. For instance, exact knowledge of both the absorbed dose to water at a specified point and its spatial distribution are of importance in radiotherapy. It is also important to the possibility of deriving the dose to an organ of interest in the patient. In this context, the most of TL phosphors are not suitable for radiation dosimetry. For a suitable radiation dosimeter purposes, TL phosphor must demonstrate the following properties [52]:

- a) Dosimeter should have to relatively simple TL glow curve and its peak temperature of main glow peak should be between 180 and 250 °C. It should be remembered that at higher temperature, the infrared emission from the hot sample and sample holder increasingly interferes with the measurement of low doses.
- b) Dosimeter should have high sensitivity, which consist of both high efficiency of light emission and low threshold dose. The desirable properties of TLD materials include a linear response to absorbed dose and an adequate sensitivity. The dose response of most TL materials is far from linear, however, monitoring a variety of non-linear effects depending upon the dose range and irradiation.
- c) Dosimeter should have high resistance against environmental factors as humidity, solvents, low fading at room temperature.
- d) Dosimeter should have low photon energy dependence of response and a linear response over high dose ranges for most application. Depending on the special

use, high or low thermal neutron sensitivity or a certain LET response may also be the wanted properties.

- e) Effective atomic number  $Z_{\text{eff}}$  of dosimeters should be close to that of biological tissue, in order to deal with a tissue equivalent material.
- f) The phosphor must be economic. It may be easier and cheaper to work with a “one way” dosimeter.
- g) It should be nontoxic.
- h) It must have not complex annealing procedure for reuse.
- i) It might be advantageous if the sample can easily be prepared with reproducible features in a normally equipped chemical laboratory [44,53]

Actually, a few of materials have the above-mentioned properties. The nominally pure compounds, such salts and oxides usually show weak TL signals and they are not considered as efficient dosimetric materials. But when they are doped with proper impurities, which act as activators of host materials, much higher efficiencies will be obtained after the doping.

#### **2.4. Types of Luminescence**

Luminescence is emission of light from a semiconductor or insulator by excitation energy. The different types of luminescence phenomena are classified according of the stimulation method causing light emission. Some of them are:

- a. Thermoluminescence : emission of light due to heating of temperature
- b. Photoluminescence : produced by stimulation with UV light;
- c. Radioluminescence : excited by ionization of radiation;
- d. Triboluminescence : stimulation due to stress of mechanic;
- e. Chemiluminescence : produced result of chemical reactions;
- f. Phosphorescence : stimulated by ionizing radiation, visible light and UV.

The process of light emission from a crystalline solid by thermal stimulation after irradiation to ionizing radiation is called as “thermally stimulated luminescence” or simply “thermoluminescence” [2]. The storage of radiation energy is an important feature for TL dosimetry. It is usually favored by presence of

activators namely impurity atoms and structural defects within the crystal structure of material. In general, the crystals may include many type of defects which can be the following types;

1. Intrinsic defects: vacancies (or missing atoms), interstitials, aggregate forms of previous defects.
2. Defects induced by ionizing radiations: F centers, V centers,  $V_k$  centers, etc.
3. Extrinsic (or impurity) defects: substitutional impurities, interstitial impurities.

The property of storing energy is because of the presence of crystal defects such as vacancies and impurities. The luminescence phenomena can be seen because of all defects can be potentially acted as traps or recombination center for charge carriers produced by suitable excitation. The defects can capture the electrons and holes produced during the irradiation process. A crystal defect is classified as a trap center if the defect is able to capture a charge carrier and reemit it back to the band it come from. A crystal defect where carriers of opposite sign can be captured, resulting in an electron-hole recombination, is classified as a recombination center. Effective thermoluminescent materials include many of traps and recombination centers, occurred by defects and impurities inside its structure [56].

## **2.5. Electronic Transitions within the Band Gap of Insulators and Semiconductors**

Theoretically, the TL is directly connected to the band structure of crystals and especially to the effects of impurities and defects within them. The energy band diagram of crystal can explain its TL properties and it can be defined by quantum mechanically [49]. In a perfect crystal, the electrons remain in the valance band (VB). The VB is separated from the conduction band (CB) by the energy band gap  $E_g$  which is called as forbidden band gap. So,  $E_g$  is energy difference between CB and VB. Figure 2.4 schematically demonstrates the energy band models, the electronic energy stages and the forbidden energy gap, and some electronic transitions in these levels [56].

There are no energy levels within the band gap for a crystal without lattice defects and impurities. The energy levels may be discrete level or may be continuously distributed level depend on the exact nature of the defects. Generally, it is known that the lattice imperfections, impurities, intrinsic and extrinsic defects can cause to the

localized energy levels within the band gap. A free electron in the CB can be attracted by a vacant anion site due to its columbic field and become trapped by them. The energy required to remove the electron from its trapping place is less than that needed to free a valance electron and so that anion vacancy has associated with it an energy level which lies somewhere between the VB and CB. The same condition is also satisfied for hole which is trapped with cation vacancies. Similar discussions apply to the incorporation of impurity ions within the crystal lattice, either in substitutional or interstitial positions. Thus, localized energy levels within the band gap can act either as traps or as recombination centers (RC). The defect where the electron is released is generally called trapping center or electron trap (ET). The defects where the electron and hole recombine is generally called recombination center (RC) or luminescent center (LC). In principle it is known that recombination centers are located near the middle of the band gap and traps are located near the edges of corresponding bands [56].

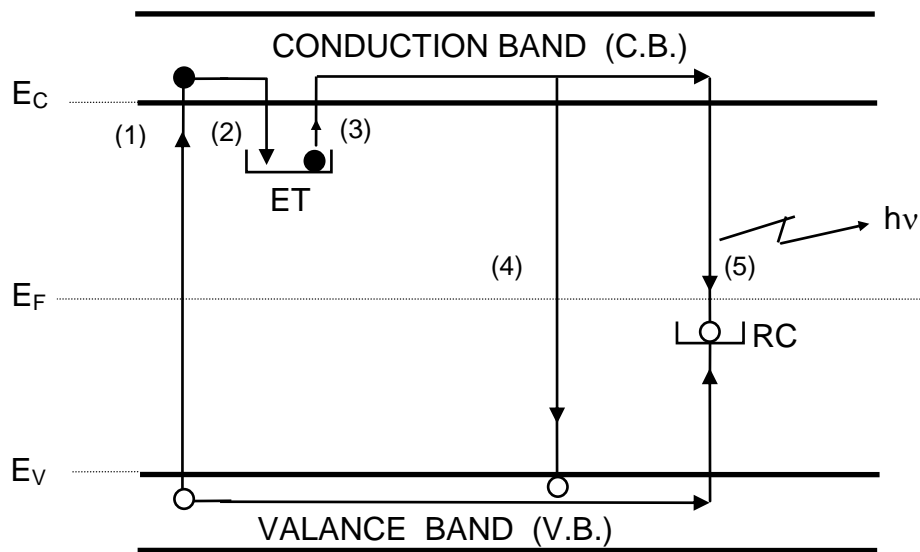


Figure 2.4: Common electronic transitions in crystalline solids: (1) ionization; (2) electron trapping; (3) electron release; (4) direct recombination; (5) indirect recombination. (ET: Electron Trap; RC: Recombination Centers) [49].

During the irradiations of crystals with high energetic radiations such as  $\alpha$ ,  $\beta$ , and  $\gamma$  correspond to the liberation of an electron from the VB into the CB remaining a hole in the VB (transition (1)). Thus, the transition (1) suitable to the process of ionization. The free electron in the CB and free hole in the VB move in the crystal up to trap at the respective lattice defects. The electron may be trapped by a transition to the

lowest available energy level at the defect (transition (2)). The hole may be trapped at a lattice defect above the valance band. The trapped electrons gain enough energy by the heating of crystal, they may be released from the traps (transition (3)) [49]. The probability of an electron being thermally released from its trap is related to Arrhenius equation ( $\exp(-E/kT)$ ). In this equation,  $E$  is called as "trap depth". It is the energy difference between the trapping level and CB.  $T$  is the temperature at which electrons are being excited from their corresponding delocalized band.

When an electron is released to the CB, it is once again become free to move through the CB and may recombine with a charge carrier of opposite sign, either directly (transition (4)), or indirectly (transitions (5)). The luminescence yields if the recombination process is accompanied by the emission of light.

The trapped electrons by traps can be released thermally into the CB by heating the crystal and then make a transition to the RC. This process is termed as the TSL. Additionally, external light exposure can release captured electrons from a trap center to the CB from where they can recombine into the RC. This process is called as optically stimulated luminescence (OSL) [49].

The experimental TL emission study can suffice a satisfactory tool to get detailed information about the trapping (kinetic) parameters. They are: the activation energy ( $E$ ), frequency factor ( $s$ ), and a kinetic order ( $b$ ) synthesizing the quality of the involved phenomena [2].

In general, the ranges of kinetic order is between 1 and 2. The former value is corresponded to a situation where an electron provides energy to rise in the CB and, consequently, to fall to a RC where it undergoes recombination with hole. The latter one stands for a situation where this phenomenon has the same probability of retrapping. Intermediate conditions are likely to occur. The mathematical models main on these definitions are including of convenient differential equations systems. The analytical forms of them are to be checked by means of suitable experimental data. It is therefore evident how the involved parameters are to be conveniently adjusted until a fair agreement between theory and practice is attained. The most promising tool is the observation and the recording of TL emission, under several experimental conditions, as a function of temperature. For a constant heating rate, these two observations are equivalent. It may be a single or multi-peaks structure and

a correspondence can be pointed out between a peak and an electron trap level. The analytical form for a single peak, which the overall curve is a superposition of, can fully defined by means of some geometrical parameters as the peak position, its left and right widths, the ratio between them, the overall width, the height. This last one is dependent on the heating rate and increases with the increasing of it.

## 2.6. The One Trap–One Recombination (OTOR) Centre Model

To explain the TL phenomenon, the basic model of band diagram must consist of a single type of electron trap (T) and a single type of recombination center (R) in the forbidden gap, as shown in Figure 2.5 [49]. It is necessary to indicate that two energy level band model is the minimum number required in order to describe the TL-process. However, the band model of an actual sample may be much more complex than this simple model. Moreover, the basic model is enough to explain the fundamental properties of TL production.

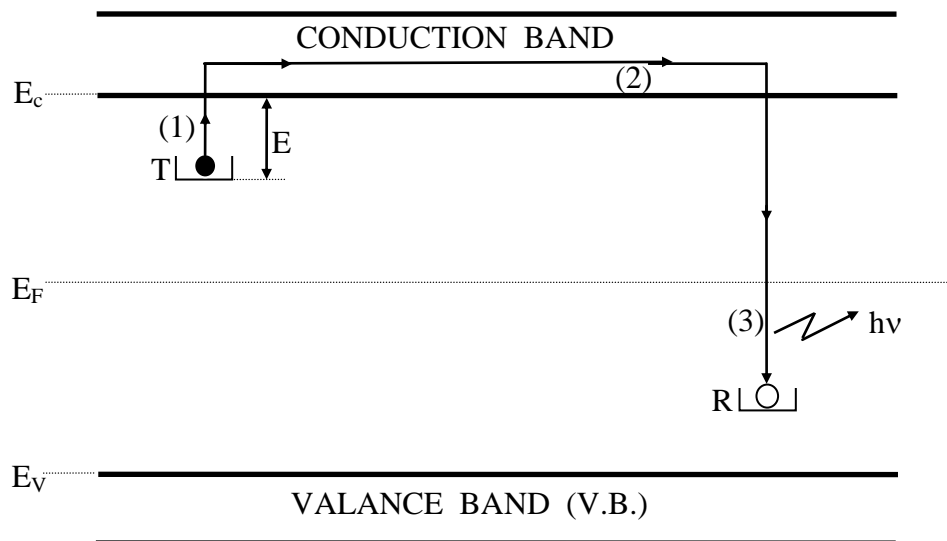


Figure 2.5: Simple band model for TL emission. Allowed transitions: (1) thermal release, (2) migration in the conduction band, (3) radiative recombination [2].

## 2.7. Trap-Filling Process

During the irradiation of crystals with ionizing radiation, the differential equations establishing the mobility of electrons between the electron trap (T), the RC and the CB are [2,49-55]:

$$\frac{dn_c}{dt} = f - n_c n_h A_h - n_c (N - n) A_n \quad (2.1)$$

$$\frac{dn}{dt} = n_c (N - n) A_n \quad (2.2)$$

$$\frac{dn_v}{dt} = f - n_v (N_h - n_h) A_m \quad (2.3)$$

$$\frac{dn_h}{dt} = n_v (N_h - n_h) A_m - n_c n_h A_h \quad (2.4)$$

The meaning of variables used in these equations is that:  $E$ =activation energy of the electron traps (in eV),  $s$ =frequency factor of the electron trap (in  $s^{-1}$ ),  $n_c$  is the number of electrons in the conduction band (per unit volume  $m^{-3}$ ),  $n_v$  is the number of holes in the valance band,  $N$  is the concentration of available electron traps (of depth  $E$  below the conduction band) in the crystal (in  $m^{-3}$ ),  $n$  is the concentration of the filled electron traps in the crystal (in  $m^{-3}$ ),  $n_h$  is the concentration of holes in the recombination centers,  $N_h$  is the concentration of available hole centers,  $A_n$  is the transition coefficient for electrons in the conduction band becoming trapped (volume/until time  $m^3sec^{-1}$ ),  $A_m$  is the transition coefficient for holes in the valance band to be trapped in the hole centers,  $A_h$  is recombination transition coefficient for electrons in the conduction band with holes in centers and  $f$  is the electron hole production rate.

## 2.8. Trap-Emptying Process

If the depth of trap is very greater than  $kT_0$  ( $E \gg kT_0$ ) where  $k$  is Boltzmann's constant which is equal to  $8.617 \times 10^{-5}$  eV/K and  $T_0$  is the irradiation temperature, the trapped electrons in traps will stay for a long time after exposure of the radiation. Because of the occurred free electrons and holes after irradiation there have to be equal number of trapped holes at RC. The normal condition of the equilibrium for Fermi level  $E_f$  is located down trapping level (T) but up level of RC. This means the populations of holes and trapped electrons show a non-equilibrium state. The reaction path for return to equilibrium is explained by the probability ( $p$ ) per unit time of release of an electron from the trap and it is given by,

$$p = s \exp\left\{-\frac{E}{kT}\right\} \quad (2.5)$$



According to this equation, the relaxation rate is slow at low temperature and the non-equilibrium state is governed by the combination of kinetic parameters  $E$  and  $s$ . The lifetime ( $\tau$ ) of the electrons in the traps at a temperature  $T$  is given by

$$\tau = p^{-1} \quad (2.6)$$

Now, if  $n$  is the number of trapped electrons in electron traps then  $n$  decreases with time  $t$  according to the following equation if the temperature is kept constant:

$$\frac{dn}{dt} = -np \quad (2.7)$$

If the above equation integrates

$$\int_{n_o}^n \frac{dn}{n} = - \int_{t_o}^t p \cdot dt \quad (2.8)$$

gets

$$n = n_o \cdot \exp \left[ -s \exp \left\{ -\frac{E}{kT} \right\} t \right] \quad (2.9)$$

where  $n_o$  is the number of trapped electrons at the initial time  $t_0 = 0$ . If the following assumptions were done:

1. The temperature is so low, no electrons are released from the traps during the irradiation of samples.
2. The electron's lifetime in the CB is too short,
3. The luminescence efficiency of recombination centers is independent of temperature,
4. The number of electron traps and recombination centers are independent of temperature.

The escape probability of electrons from the traps can be speeded up by increasing the temperature of the TL material above irradiation temperature  $T_0$ . As mentioned previously, the electrons will now be released from the trap into the CB with increasing temperature. Then, they move through the CB of the crystal until they undergo recombination at the RC or retrapping by the electron traps. In the simple model, when the electron captured by RC, it passes one of the higher excited states of RC and then return to the ground state by the emission of light quanta in the visible region of electromagnetic spectrum. The TL intensity  $I(t)$  of photons per per unit time  $t$  during heating is proportional to the rate of recombination of holes and electrons at the recombination center. Now, let us assume that  $m$  ( $\text{m}^{-3}$ ) is the

concentration of holes that are capture by recombination centers, then the equation intensity of TL can be written as

$$I(t) = -\frac{dm}{dt} \quad (2.10)$$

In here, it was assumed that each recombination produces a visible photon and all of the emitted photons recorded by the photomultiplier tube of TLD reader. The rate of recombination of holes and electrons will be proportional to the number of free electrons  $n_c$  in the CB and the number of holes  $m$  in the RCs,

$$I(t) = -\frac{dm}{dt} = n_c mA_h = n_c (n + n_v) A_h \quad (2.11)$$

In here, the constant  $A_h$  is the recombination possibility that is said to be in units of volume per unit time and it is assumed to be temperature independent. The rate of change of the concentration of trapped electrons  $n$  in the electron traps is equal to the rate of thermal release minus the rate of retrapping,

$$-\frac{dn}{dt} = np - n_c (N - n) A_n = ns \exp\left\{-\frac{E}{kT}\right\} - n_c (N - n) A_n \quad (2.12)$$

where  $N$  is the concentration of electron traps and  $A_n$  is the probability of retrapping ( $m^3/s$ ). Similarly, the rate concentration of free electrons in the CB is equal to the rate of thermal release minus the rate of retrapping and the rate of recombination,

$$\frac{dn_c}{dt} = ns \exp\left\{-\frac{E}{kT}\right\} - n_c (N - n) A_n - n_c mA_h \quad (2.13)$$

The equations between 2.11 and 2.13 are called as the charge carrier traffic's equations in the OTOR model. These equations are the basis of many analyses of TL phenomena. The equation (2.12) express mathematically the fact that electrons in the trap can be either thermally excited in the conduction band ( $ns \exp\{-E/kT\}$ ) or they can be retrapped in the trap with a probability coefficient  $A_n(n_c(N-n))$ . The equation (2.13) shows the change the number of electrons  $n_c$  in the CB. The free electrons in the CB can be reduced by either trafficking into the trap ( $-dn/dt$ ), or by recombination in the RC with a probability coefficient  $A_h(-A_h n_c(n+n_c))$ . The equation (2.11) defines the rate of change of the number of holes trapped in the RC and the right-hand side representing the rate of change of the total number of electrons in the crystal. Unfortunately, it is not analytical solutions of these equations. To solve them,

some simplifying assumptions must be additionally required. One of the important approximation is

$$\left| \frac{dn_c}{dt} \right| \ll \left| \frac{dn}{dt} \right|, \quad \left| \frac{dn_c}{dt} \right| \ll \left| \frac{dm}{dt} \right| \quad (2.14)$$

This approximation is called the quasi-equilibrium assumption [3], because of it requires that the free electron concentration in the conduction band is quasi-stationary. Because of charge neutrality during the irradiation of crystal

$$n_c + n = m \quad (2.15)$$

Now, if the quasi-equilibrium is applied in above equation ( $n_c \approx 0$  means that  $n \approx m$ )

$$I(t) = -\frac{dm}{dt} \approx -\frac{dn}{dt} \quad (2.16)$$

Since  $dn_c/dt \approx 0$  one gets from equation (2.11) and (2.12):

$$I(t) = \frac{mA_n ns \exp\left\{-\frac{E}{kT}\right\}}{(N-n)A_h + mA_n} \quad (2.17)$$

## 2.9. First-order kinetics

Although the equation (2.17) cannot be solved analytically without additional simplifying approximation; Randall and Wilkins [58-59] applied another approximation and they have assumed negligible retrapping during the heating stage (i.e.  $mA_n \gg (N-n)A_h$ ). After this approximation, Eqn.(2.17) can be rewritten as

$$I(t) = -\frac{dn}{dt} = sn \exp\left\{-\frac{E}{kT}\right\} \quad (2.18)$$

This differential equation defines the charge carrying process in the lattice as a first-order ( $b=1$ ) process and the calculated glow peaks from this equation are called first-order glow peaks. Its solution yields

$$I(t) = -\frac{dn}{dt} = n_0 s \exp\left\{-\frac{E}{kT}\right\} \exp\left\{-s \int_0^t \exp\left\{-\frac{E}{kT(t')}\right\} dt'\right\} \quad (2.19)$$

In here,  $n_0$  is the total number of trapped electrons in traps at time  $t = 0$ . When the temperature is increased as a linear function of time according to following equation

$$T(t) = T_0 + \beta t \quad (2.20)$$

where  $\beta$  is the constant heating rate and  $T_0$  is the temperature at  $t=0$ . If the above equation can be written as  $\beta=dT/dt$  and then introduces it into equation (2.14)

$$\int_{n_0}^n \frac{dn}{n} = -\left(\frac{s}{\beta}\right) \int_{T_0}^T \exp\left(-\frac{E}{k.T'}\right) dT' \quad (2.21)$$

It gives the number of trapped electrons ( $n$ ) in terms of  $\beta$  as

$$n = n_0 \cdot \exp\left[-\left(\frac{s}{\beta}\right) \int_{T_0}^T \exp\left(-\frac{E}{k.T'}\right) dT'\right] \quad (2.22)$$

Then, the first-order TL equation is obtained as a function of temperature in the following form

$$I(T) = -\frac{1}{\beta} \frac{dn}{dt} = n_0 \frac{s}{\beta} \exp\left\{-\frac{E}{kT}\right\} \exp\left\{-\frac{s}{\beta} \int_{T_0}^T \exp\left\{-\frac{E}{kT'}\right\} dT'\right\} \quad (2.23)$$

This is the well-known Randall–Wilkins first-order equation. According to this equation, the peak has a characteristic asymmetric shape being wider on the low temperature side than on the high temperature side. In the initial rise of low temperature side of this glow peak, the intensity of TL is dominated by the first exponential ( $\exp(-E/kT)$ ). Thus, when  $I$  is plotted as function of  $1/T$ , a straight line is expected in the initial rise temperature range, with the slope of  $-E/k$ . Then, the activation energy  $E$  is readily found using the slope of graph.

The properties of first-order TL equation are represented in Figure 2.6. In Figure 2.6(a) it is shown how  $I(T)$  varies with  $n_0$  from  $0.25 \text{ m}^{-3}$  up to  $2 \text{ m}^{-3}$ , while  $E=1 \text{ eV}$ ,  $s=1.0 \times 10^{12} \text{ s}^{-1}$  and  $\beta=1 \text{ K/s}$  are all kept constant. As seen the temperature  $T_m$  at the peak maximum remains constant with  $n_0$ . This is properties of all first-order TL glow peaks. The condition for the maximum can be found by setting  $dI/dt=0$  (or, somewhat easier from  $d \ln I(T)/dt=0$ ).

$$\frac{\beta E}{kT_m^2} = s \exp\left\{-\frac{E}{kT_m}\right\} \quad (2.24)$$

In this equation,  $n_0$  does not appear. Because,  $T_m$  does not depend on  $n_0$ . Figure 2.6(a) further represented that not only the peak height  $I_m$  at the peak maximum but each point on the curve is proportional to  $n_0$ . In the dosimetric applications,  $n_0$  is the very important parameter. Because, this parameter is proportional to the absorbed dose. To obtain  $n_0$  then absorbed dose, the area under the glow peak is enough which is equal to  $n_0$

$$\int_0^\infty I(t) dt = -\int_0^\infty \frac{dn}{dt} dt = -\int_{n_0}^{n_\infty} dn = n_0 - n_\infty \quad (2.25)$$

and  $n_\infty$  is zero while  $t \rightarrow \infty$ . Figure 2.6(b) shows variation of activation energy  $E$  from 0.8 to 1.2 eV. As seen, when  $E$  increases the peak temperature shifts to higher sides with a decrease in the peak height and an increase in the width covering the area (i.e.  $n_0$ ) constant.

Figure 2.6(c) shows the similar changes of frequency factor  $s$  with increasing from  $10^{11}$  to  $10^{14} \text{ s}^{-1}$ . But now in the opposite way: as  $s$  increases the peak temperatures shifts to lower temperature sides with an increase of the peak height and a decrease in peak-width. Figure 2.6(d) shows the effects of the heating rates on the first-order glow peaks. As seen, when  $\beta$  increases the peak shifts to higher temperatures while the height decreases.

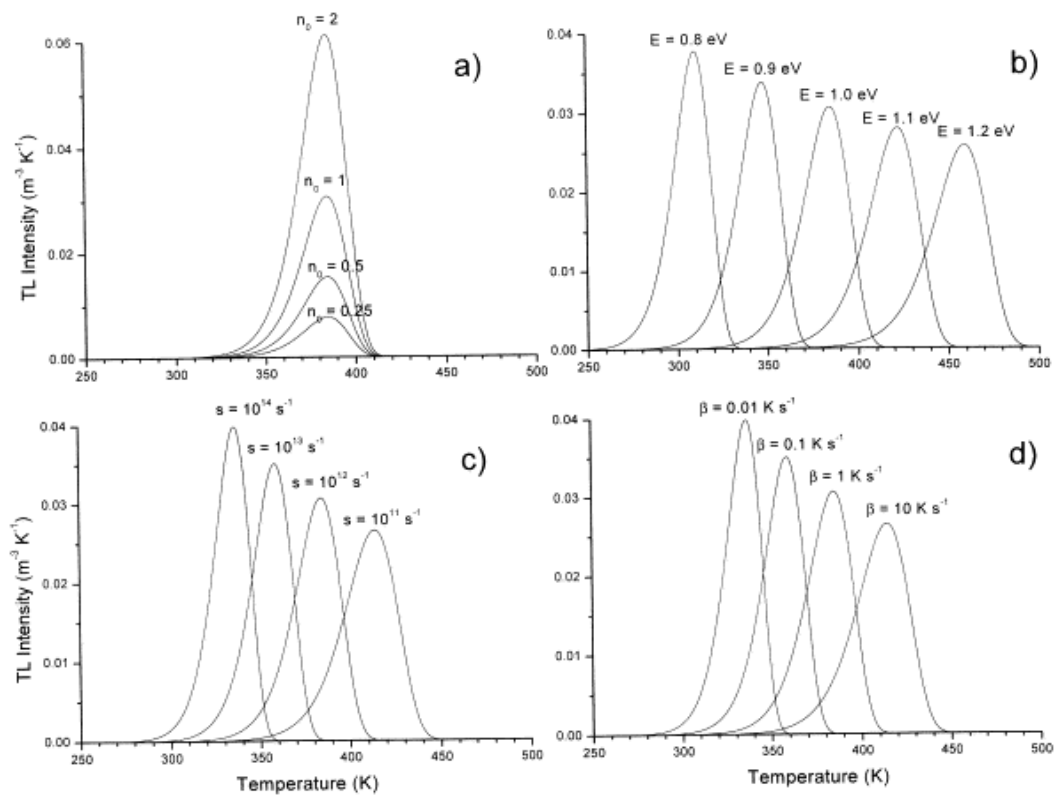


Figure 2.6: Properties of the Randall–Wilkins first-order TL equation, showing: (a) variation with  $n_0$ , the concentration of trapped charge carriers after irradiation; (b) the variation with  $E$ , the activation energy; (c) the variation with  $s$ , the escape frequency; (d) the variation with  $\beta$ , the heating rate. Parameter values:  $n_0=1 \text{ m}^{-3}$ ;  $E=1 \text{ eV}$ ;  $s=1 \times 10^{12} \text{ s}^{-1}$ ,  $\beta=1 \text{ K/s}$  of which one parameter is varied while the others are kept constant [58].

As mentioned previously, the two parameters the activation energy  $E$  and the frequency factor  $s$  are the basic physical parameters. The other two parameters can be obtained by the experimenter by choosing a certain dose ( $n_0$ ) and by read-out of the signal at a certain heating rate  $\beta$ .

The analytical solution of equation (2.23) is not possible due to the integral on the right hand side of this equation. But, using series expansion, it can be calculated as partial integral by each part to be equal to [61]

$$F(T, E) = T \exp(-E/kT) \sum_{n=1}^{\infty} \left( \frac{kT}{E} \right)^n (-1)^n n! \quad (2.26)$$

If the first two terms were only chosen, the integral can be converted as following

$$F(T, E) = \frac{kT^2}{E} \exp(-E/kT) \left( \frac{1-2kT}{E} \right) \quad (2.27)$$

In practical applications it is convenient to indicate the glow peak as parameters which are easy to derive experimentally, namely the intensity of peak at the maximum  $I_m$  and the temperature at the maximum  $T_m$ . Therefore, by the solution of this integral and for condition of the maximum temperature the following TL intensity equation (2.24), Kitis et al. [62] have shown that Eqn.(2.23) can be quite accurately approximated by

$$I(T) = I_m \exp \left[ 1 + \frac{E}{kT} \frac{T - T_m}{T_m} - \frac{T^2}{T_m^2} \exp \left\{ \frac{E}{kT} \frac{T - T_m}{T_m} \right\} (1 - \Delta) - \Delta_m \right] \quad (2.28)$$

with  $\Delta = 2kT/E$  and  $\Delta_m = 2kT_m/E$ . On the other hand, by keeping a lot of terms in the above approximation, Bos et.al. [63] were approximated the first-order TL glow curve expression in the following form,

$$I(T) = n_0 s \exp\left(-\frac{E}{kT}\right) \exp \left[ \left( -\frac{s kT^2}{\beta E} \exp\left(-\frac{E}{kT}\right) \right) * (0.9920 - 1.620 \frac{kT}{E_a}) \right] \quad (2.29)$$

## 2.10. Second-order kinetics

Garlick and Gibson [64] considered the possibility of retrapping of electrons in the CB by electron traps, (i.e.  $m A_n \ll (N-n) A_h$ ). In addition, if the electron is far from saturation, i.e.  $N \gg n$  and  $n=m$ , the equation (2.17) becomes

$$I(t) = -\frac{dn}{dt} = s \frac{A_n}{N A_h} n^2 \exp \left\{ -\frac{E}{kT} \right\} \quad (2.30)$$

As seen,  $dn/dt$  is proportional to  $n^2$  in this equation. This means that it is a second-order reaction. With the additional assumption of equal probabilities of recombination and retrapping,  $A_n = A_h$ , the above equation becomes

$$I(T) = \frac{n_0^2}{N} \frac{s}{\beta} \exp \left\{ -\frac{E}{kT} \right\} \left[ 1 + \frac{n_0 s}{N \beta} \int_{T_0}^T \exp \left\{ -\frac{E}{kT'} \right\} dT' \right]^{-2} \quad (2.31)$$

This is well-known second-order TL equation of the Garlick–Gibson. The main property of its graph is that it is nearly symmetric, with the higher temperature from the half of the curve slightly wider than the lower temperature half. It can be understood from the consideration of the fact that in a second-order reaction significant concentrations of released electrons are retrapped before they recombine. In this way, it is giving rise to a delay in the luminescence emission and spreading out of the getting off over a wider temperature range.

In the second-order kinetic, the initial concentration  $n_0$  seems not constant as in the first-order case with the variation of dose levels. Its graph is represented in Figure 2.7(a). As seen that  $T_m$  decreases as  $n_0$  increases. The temperature shift can be approached by [21]

$$T_1 - T_2 \approx T_1 T_2 \frac{k}{E} \ln f \quad (2.32)$$

where  $T_1$  is the peak temperature at peak intensity at a certain dose level and  $T_2$  the peak temperature at peak intensity after  $f$  times higher dose. When using the parameters in Figure 2.7(a), it was calculated as the shift in the peak temperatures is 25 K. When  $E=1$  eV,  $T_1=400$  K and the absorbed dose is increased by a factor 1000, which is easy to realize experimentally, a temperature shift of 77 K can be expected. From equation (2.32) it follows further that for a given increase of the dose the shallower the trap, i.e., the smaller  $E$ , the larger the peak shift. Figure 2.7(b) illustrates the change in size and position of a second-order peak as function of  $E$ , in Figure 2.7(c) as function of  $s/N$ , and in Figure 2.7(d) as function of the heating rate. The area under the curve is, as in the situation of first-order kinetics, proportional to the initial concentration  $n_0$  but the peak height is no longer directly proportional to the peak area, although the deviation is small.

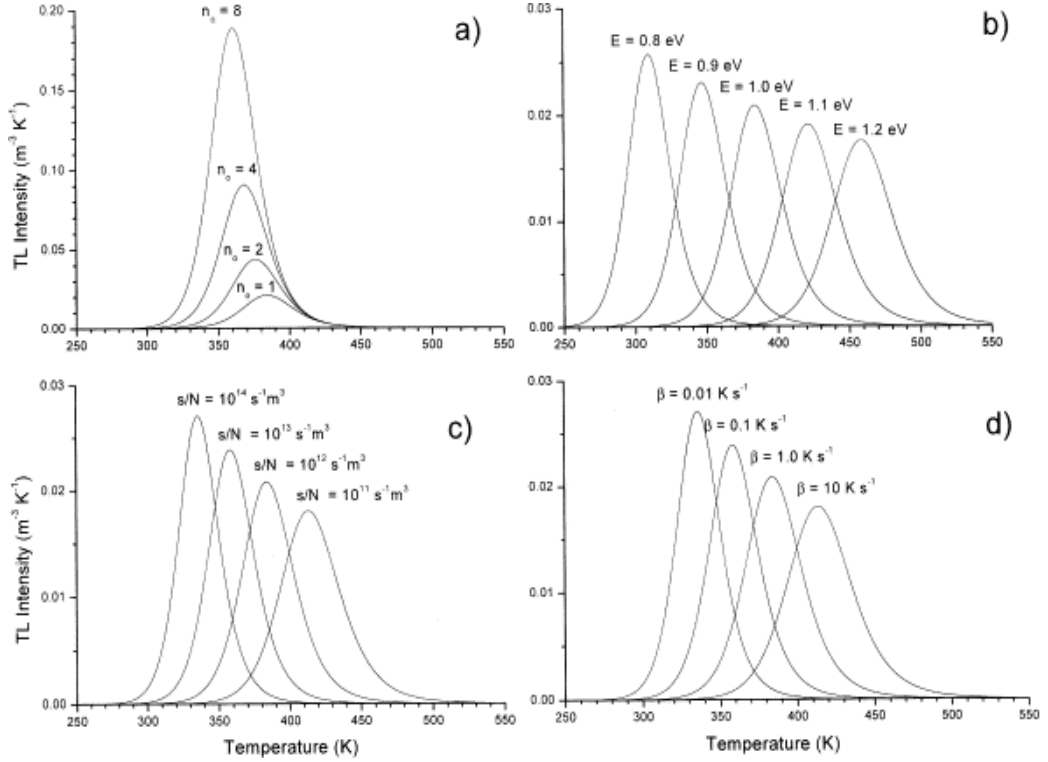


Figure 2.7: Properties of the Garlick–Gibson second-order TL equation, showing: (a) variation with  $n_0$ , the concentration of trapped charge carriers after irradiation; (b) the variation with  $E$ , the activation energy; (c) the variation with  $s/N$ ; (d) the variation with  $\beta$ , the heating rate. Parameter values:  $n_0=1 \text{ m}^{-3}$ ;  $E=1 \text{ eV}$ ;  $s/N=1 \times 10^{12} \text{ s}^{-1} \text{ m}^3$ ,  $\beta=1 \text{ K/s}$  of which one parameter is varied while the others are kept constant [64].

Also the glow peak shape for second-order kinetics, the equation (2.31) can be approximated and written as with a function of maximum peak intensity  $I_m$  and  $T_m$  [18]

$$I(T) = 4I_m \exp\left(\frac{E}{kT} \frac{T - T_m}{T_m}\right) \times \left[ \frac{T^2}{T_m^2} (1 - \Delta) \exp\left\{ \frac{E}{kT} \frac{T - T_m}{T_m} \right\} + 1 + \Delta_m \right]^{-2} \quad (2.33)$$

with  $\Delta$  and  $\Delta_m$  the same meaning as in Equation(2.28).

## 2.11. General-order kinetics

The first- and second-order forms of the TL equation derived after the specific approximations. However, if these assumptions do not hold, the TL peaks will fit neither first- nor the second-order kinetics. Therefore, May and Partridge [66] considered this situation and used another empirical equation to obtain general-order TL equation,



$$I(t) = -\frac{dn}{dt} = n^b s' \exp\left\{-\frac{E}{kT}\right\} \quad (2.34)$$

where  $s'$  is called as pre-exponential factor and its dimension is  $m^{3(b-1)}/s$  and  $b$  is defined as the general-order parameter and varies between 1 and 2, not necessarily just equal to 1 or 2. Integration of above equation (2.34) for  $b \neq 1$  results

$$I(T) = \frac{s''}{\beta} n_0 \exp\left\{-\frac{E}{kT}\right\} \left[ 1 + (b-1) \frac{s''}{\beta} \int_{T_0}^T \exp\left\{-\frac{E}{kT'}\right\} dT' \right]^{-b/(b-1)} \quad (2.35)$$

where now  $s'' = s' n_0^{b-1}$  with unit  $s^{-1}$ . Equation (2.35) goes to the second-order equation when  $b=2$  and decreases to equation (2.23) when  $b \rightarrow 1$ . It have to be noted that according to Equation (2.34) the dimension of  $s'$  have to be  $m^{3(b-1)} s^{-1}$  that is meaning that the dimension changes with the order  $b$  which makes it difficult to interpret physically. However, the general-order case is still useful since intermediate cases can be dealt with and it smoothly goes to first- and second-orders when  $b \rightarrow 1$  and  $b \rightarrow 2$ , respectively (see Figure 2.8).

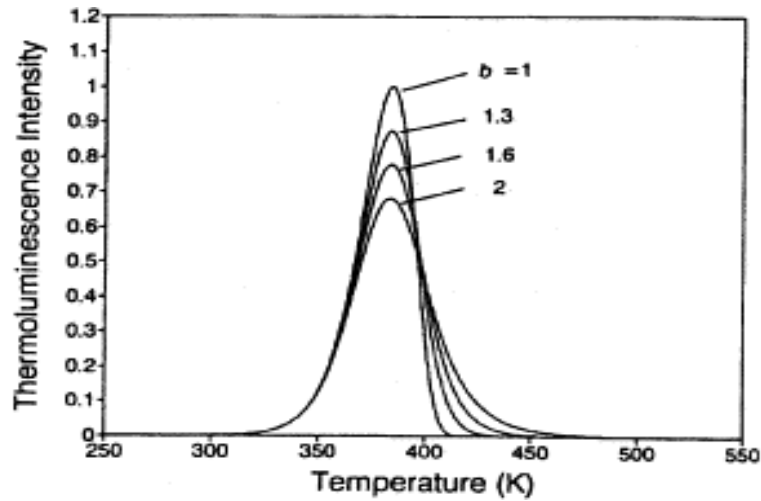


Figure 2.8: Comparison of first-order ( $b=1$ ), second-order ( $b=2$ ) and intermediate-order ( $b=1.3$  and  $1.6$ ) TL peaks, with  $E=1$  eV,  $s=1 \times 10^{12} s^{-1}$ ,  $n_0=N=1 m^{-3}$  and  $\beta=1$  K/s [49].

In this model, the glow curve can also be approximated by using the following equation,

$$I(T) = n_0 s \exp\left(-\frac{E}{kT}\right) \left[ 1 + \left(-\frac{(b-1)s kT^2}{\beta E} \exp\left(-\frac{E}{kT}\right) * (0.9920 - 1.620 \frac{kT}{E})\right) \right]^{\frac{b}{b-1}} \quad (2.36)$$

## **2.12. Trapping Parameters Determination Methods**

The determination of trapping parameters from thermoluminescence glow curves has been a subject of interest for half a century. There are many different methods to find the trapping parameters by using the glow curves [2, 49,57 68-71]. Some of them are initial rise (IR), variable heating rate (VHR), two heating rate, isothermal decay (ID), peak shape (PS), partial thermal cleaning (PTC) and peak area (PA) methods.

If any glow peak is highly isolated from the others, the experimental methods such as initial rise, variable heating rates, isothermally decay, and peak shape methods are suitable methods to demonstrate these parameters. However, the glow curve includes of several glow peaks in most TL samples. In situation of overlapping glow peaks there are essentially two ways to get these parameters, the first one is the partial thermal cleaning method and the second one is the computer glow curve deconvolution method. In many situations, the partial thermal cleaning method cannot be applied to completely isolate the peak of interest without any perturbation on it. Therefore, the computer glow curve deconvolution (CGCD) program has become very popular method to evaluate trapping parameters from TL glow curves [54,63].

### **2.12.1. CGCD Method**

It can be remembered from previous parts, the computer glow curve deconvolution (CGCD) is one of the most important methods to show trapping parameters from TL glow curves. By the using it, many overlapping glow peaks can be separated without heating and addition dose.

The CGCD is the method which is famous and one of the powerful methods in the study of TL [2]. This method is especially used in the dosimetric studies of TL samples. The application of the CGCD method for the decomposition of a composite TL glow curve into its individual glow peaks is widely used since 1970 [73-73,76]. On the other hand, the obtained results from this method are highly dependent upon the input parameters that used in the deconvolution program. For example, it is very important to correctly decide how many glow peaks there are in the glow curve structure during the analyses of the complex glow curves by CGCD program and which of them have first- or general-order kinetics. In some cases, the best-fits can be obtained when different number of peaks is used in the curve fitting program

instead of real number of glow peaks to be in the glow curve. Therefore, it should be necessary to decide the correct number of glow peaks and their kinetic orders in the glow curve of studied samples in this thesis.

In this research, the analyze of the glow curves was done by using the CGCD program. The program was developed at the Reactor Institute at Delft, The Netherlands [63]. This program is capable of simultaneously deconvolution as many as nine glow peaks from glow curve. Two different equations were used in the computer program. In the first equation, the glow curves are approximated from first-order TL kinetic,

$$I(T) = n_0 s \exp\left(-\frac{E}{kT}\right) \exp\left[ \left(-\frac{s kT^2}{\beta E} \exp\left(-\frac{E}{kT}\right) * (0.9920 - 1.620 \frac{kT}{E_a})\right) \right] \quad (2.29)$$

In the second equation, the glow curves are approximated with general-order TL kinetics,

$$I(T) = n_0 s \exp\left(-\frac{E}{kT}\right) \left[ 1 + \left(-\frac{(b-1)s kT^2}{\beta E} \exp\left(-\frac{E}{kT}\right) * (0.9920 - 1.620 \frac{kT}{E_a})\right) \right]^{\frac{b}{b-1}} \quad (2.36)$$

The summation of overall peaks and background contribution can lead to composite glow curve formula as shown below

$$I(T) = \sum_{i=1}^n I_i(T) + a + b \exp(T) \quad (2.37)$$

where  $I(T)$  is the fitted total glow curve,  $a$  allows for the electronic noise contribution to the planchet and dosimeters infrared contribution to the background.

Starting from the above equation (2.37), the least square minimization procedure and figure of merit (FOM) [74-75] was used to judge the fitting results as to whether they are good or not. i.e.

$$FOM = \sum_{i=1}^n \frac{|N_i(T) - I(T)|}{A} = \sum_{i=1}^n \frac{|\Delta N_i|}{A} \quad (2.38)$$

where  $N_i(T)$  is the  $i$ -th experimental points (total  $n=200$  data points),  $I(T)$  is the  $i$ -th fitted points, and  $A$  is the integrated area of the fitted glow curve.

From many experiences [74-75], it can be said that if the values of the FOM are between 0.0% and 2.5%, the fit is good; if the values of the FOM are between 2.5% and 3.5%, the fit is fair; and if the FOM values are greater than 3.5%, the fit is bad. To have a graphic representation of the agreement between the experimental and fitted glow curves, the computer program also plots the function,

$$X(T) = \frac{N_i(T) - I_i(T)}{\sqrt{I_i(T)}} \quad (2.39)$$

which is a normal variable with an expected value 0 and  $\sigma=1$  where  $\sigma^2(T)=I_i(T)$ .

### 2.12.2. Initial Rise Method

According to this method, the initial rise part of a TL curve is exponentially dependent on temperature according to

$$I(T) = C \exp(-E/kT) \quad (2.40)$$

where the C is a constant and the other parameters have usual meaning. This expression can be understood by examination of any equations (2.18), (2.30) or (2.34) or in which it can be seen that if the temperature to which the sample is heated is low enough for  $n$  to be approximately constant (i.e., for very little detrapping to have taken place). In this case, the equations become independent of kinetics and the equation 2.40 naturally emerges from them. Clearly then, if a plot  $\ln(I)$  versus  $1/T$  is made over this initial region, then a straight line of slope  $-E/k$  is obtained, from which the activation energy  $E$  is easily found. That is why it is probably to evaluate  $E$  not including any data of the frequency factor  $s$  by uses of equation

$$E = -kd(\ln(I)) / d(1/T) \quad (2.41)$$

In this method,  $n$  should be stayed approximately constant. An increase in temperature beyond a critical value ( $T_c$ ), this approximation becomes invalid. Therefore, the IR method can only be used when the glow peak is well defined and clearly separated from the other peaks. To get rid of from this problem, several methods of glow peak separation have been devised. The most popular of them is the “thermal cleaning” method. In this way, the specimen is first heated to a temperature just beyond the maximum of the first peak in the glow curve, thus largely emptying the traps supplied to this peak. Then, the specimen is quickly cooled to room temperature (RT) and then it is reheated up to end of the temperature to record remaining part of glow curve. Then the sample is again irradiated at the same level in previous irradiation and it is heated to a temperature just beyond the first reading, and it is again cooled to RT and so on from beginning to end the whole glow curve. As a result, the critical temperature is increased step by step after each repeated experiment and a series of glow curves were recorded after each experiment. However, there is always the danger that the preceding peak will not have been completely removed if the glow peaks are highly overlapped. Due to highly

overlapping glow peaks, the preceding peak cannot be probably cleaned. In this case, the cleaning cycles to produce a method of analysis which enables the trap energy distribution and at the same time to determine number of glow peaks, the critical temperature is raised by only a little change (a few degrees), so there will be very little change in  $n$  during the cooling as well, then there will be little difference in intensity between the heating and cooling cycles. The whole thermoluminescent may be excited by repeatedly heating and cooling the sample in small cycles, but many times, and, from the slope of the heating and cooling curves, the average depth of the traps being emptied during each temperature cycle may be determined. Clearly, the smaller the temperature raise on each heating, the closer the two slopes will be and so more precise will be the calculated value of  $E$ . Once the value of  $E$  was determined, the frequency factor ( $s$ ) was obtained from the equation

$$\frac{\beta E}{kT_m} = s \exp\left(-\frac{E}{kT}\right) \quad (2.42)$$

where  $T_m$  is the temperature at the maximum intensity.

### 2.12.3 Heating Rate Method

To determine the activation energy, another important method is the various heating rate method. Changing the heating rate while keeping the heating function linear, the shape of the TL peak alters and, in particular, the maximum peak temperature  $T_m$  increases with increasing heating rate. For example, if a sample is heated at two different linear heating rates  $\beta_1$  and  $\beta_2$ , the peak temperatures will be different. Therefore, the equation (2.42) can be written for each heating rate and dividing the equation for  $\beta_1$  (and  $T_{m1}$ ) by the equation for  $\beta_2$  (and  $T_{m2}$ ) and rearranging, one gets an explicit equation for the calculation of  $E$

$$E = k \frac{T_{m1} T_{m2}}{T_{m1} - T_{m2}} \ln\left[\left(\frac{\beta_1}{\beta_2}\right) \left(\frac{T_{m2}}{T_{m1}}\right)^2\right] \quad (2.43)$$

The major advantage of the heating rate method is that it only needs data to be used at a peak maximum ( $T_m, I_m$ ). Thus, if a large peak surrounded by smaller peaks, its peak temperature can be reasonably obtained from the glow curve and then the activation energy of this peak is easily obtained by this technique. In addition, the calculation of  $E$  is not effected by problems because of thermal quenching, as with the initial rise method. However, to determine the activation energies of the smaller

peaks by this method, it becomes a difficult technique to use. To do this, the thermal cleaning method might separate the satellite peaks from the others to determine its peak temperature  $T_m$  but  $I_m$  has not been affected by the cleaning process, and then its activation energy will be determined. Similar discussions apply when two (or more) peaks so closely overlapping that they appear as one composite peak [67]. When various heating rates for the first-order kinetics are used, the following equation is obtained:

$$\ln\left(\frac{T_m^2}{\beta}\right) = \left(\frac{E}{k}\right)\left(\frac{1}{T_m}\right) + \text{constant} \quad (2.44)$$

A plot of  $\ln(T_m^2/\beta)$  versus  $(1/T_m)$  should yield a straight line with a slope  $E/k$ , then  $E$  is found. Additionally, extrapolating to  $1/T_m = 0$ , a value for  $\ln(sk/E)$  is obtained from which  $s$  can be calculated by inserting the value of  $E/k$  calculated from the slope. The various heating rate method is applicable for general-order kinetics. For the general order case, one can plot  $\ln\left[I_m^{b-1}(T_m^2/\beta)^b\right]$  versus  $1/T_m$ , whose slope is equal to  $E/k$ .

#### 2.12.4. Peak Shape Methods

In this method, it is based on the shape of the peak utilize just two or three points from the glow-curve. Usually, these are the maximum of the peak  $T_m$  and either, or both, the low-and high-temperature half heights at  $T_1$  and  $T_2$ . The evaluation of  $E$  from the shape of the peak utilizing parameters such as  $T_m$ , full-width at half-maximum (FWHM)  $\omega = T_2 - T_1$ , half-width on the high temperature side of the maximum  $\delta = T_2 - T_m$ , half-width on the low-temperature side of the maximum  $\tau = T_m - T_1$ , and  $\mu_g = \delta/\omega$  called the shape parameter. Figure 2.9 shows properties of a single glow-peak, in which the peak shape method is based.

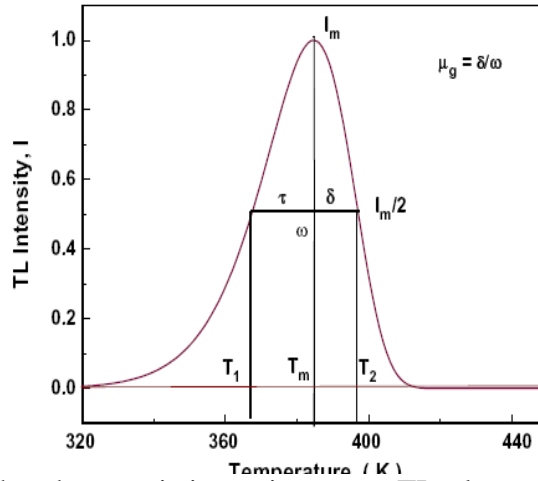


Figure 2.9: The characteristics points on a TL glow-peak, which define the peak-shape parameters [77].

The order of kinetics  $b$  can be estimated by means of shape parameters. Chen [73] found that  $\mu_g$  is not sensitive to changes in  $E$  and  $s$ , but it changes with the order of kinetics  $b$ . It has been shown that the ranges of  $\mu_g$  change from 0.42 for  $b=1$  to 0.52 for  $b=2$  in case of linear heating (Figure 2.10).

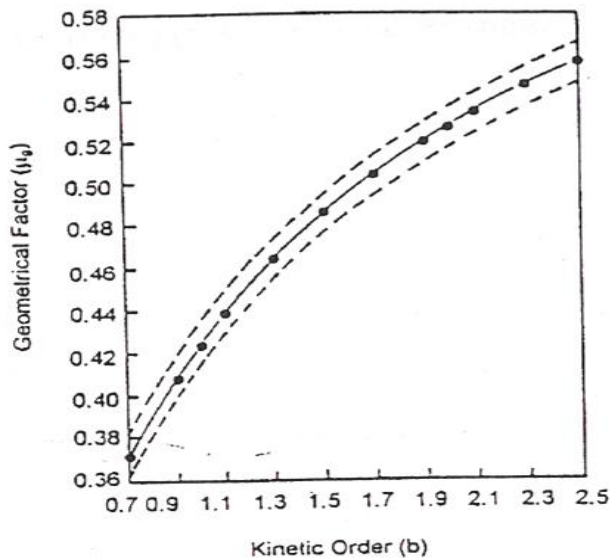


Figure 2.10: Geometrical factor ( $\mu_g$ ) as a function of the given order. [49]

The first peak-shape method was improved by Grossweiner [69]; later Chen [68] rearranged and changed Halperin and Braner's equations [70] for calculating  $E$  values;

$$\begin{aligned}
E_{\tau} &= [1.51 + 3(\mu_g - 0.42)] \frac{kT_m^2}{\tau} - [1.58 + 4.2(\mu_g - 0.42)] 2kT_m \\
E_{\delta} &= [0.976 + 7.3(\mu_g - 0.42)] \frac{kT_m^2}{\delta} \\
E_{\omega} &= [2.52 + 10.2(\mu_g - 0.42)] \frac{kT_m^2}{\omega} - 2kT_m
\end{aligned} \tag{2.45}$$

After calculation of the activation energy and the order of kinetics, using the following equations the frequency factor  $s$ , it must be noted that this parameter called as pre-exponential factor in the general order kinetic, can be estimated for first and general order kinetics respectively.

$$\begin{aligned}
s &= \frac{\beta E}{kT_m^2} \exp\left[\frac{E}{kT_m}\right] \\
s &= \frac{\beta E}{kT_m^2} \left[ \exp\left(-\frac{E}{kT_m}\right) \left(1 + (b-1) \frac{2kT_m}{E}\right) \right]^{\frac{b}{b-1}}
\end{aligned} \tag{2.46}$$

## CHAPTER 3

### EXPERIMENTAL PROCEDURE

The materials, equipments and experimental procedures utilized in this work are described in below.

#### 3.1. Synthesis of Samples

All samples were growth by spontaneous crystallization in oxygen atmosphere. To dope  $\text{Sr}_2\text{P}_2\text{O}_7$  by CuO and rare earth oxides using a solid state heating method, the desired quantities of initial reactants were weighed separately and crushed well in agate mortar [1]. The doping was done by mixing previously produced pure  $\text{Sr}_2\text{P}_2\text{O}_7$  with 5% CuO and 0.5%, 1%, 2%, 3%, 4%, 5%, 10% and 15% (by weight)  $\text{Pr}_6\text{O}_{11}$ . Then they were transferred into alumina ceramic crucibles and heated at  $900\text{ }^\circ\text{C}$  for 10h in a muffle furnace. The solid state reactions have been carried out in air with the aid of muffle furnaces.



The structural analysis of polycrystalline samples and the effect of doping on the structure of pure strontium pyrophosphates were checked by X-ray powder diffraction (XRD). The powder XRD patterns were recorded from  $5^{\circ} < 2\theta < 70^{\circ}$ , using monochromatic  $\text{CuK}\alpha$  (30 kV, 15 mA,  $\lambda = 1.54051 \text{ \AA}$ ) radiation at room temperature on a Rigaku X-ray diffractometer. The measurements were performed with  $0.05^{\circ}$  step and at  $1^{\circ}/\text{min}$  rate. The divergence slit was variable and scattering and receiving slits were  $4.2^{\circ}$  and  $0.3 \text{ mm}$ , respectively. The precise peak positions were determined by means of the fitting program CELREF [76], yielding the least squares refinement of the lattice parameters.  $\text{Sr}_2\text{P}_2\text{O}_7$  was synthesized at the same experimental conditions and indexed with respect to JCPDS Card No: 24-1011. The XRD pattern of pure  $\text{Sr}_2\text{P}_2\text{O}_7$  is given in Figure 3.1 and it was confirmed that the compound formed was  $\text{Sr}_2\text{P}_2\text{O}_7$  in an orthorhombic structure.

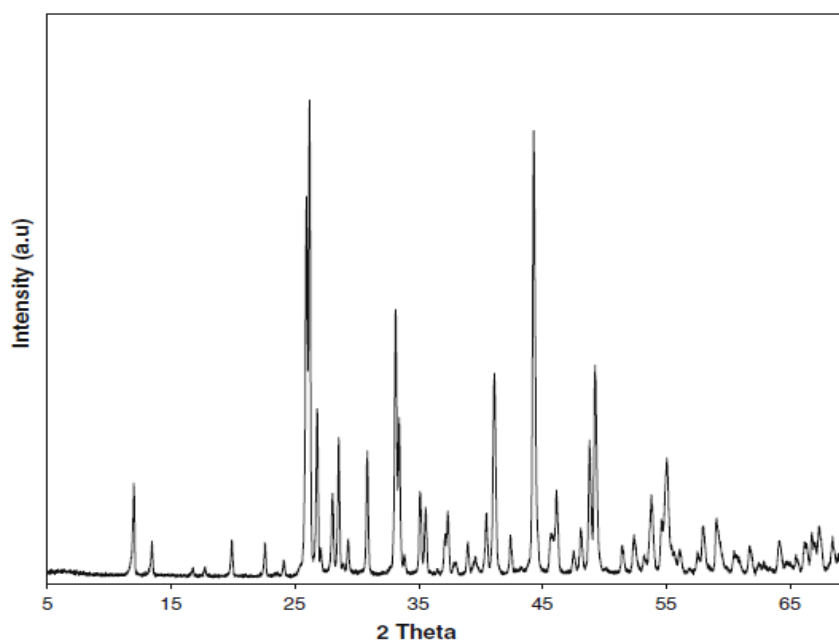


Figure 3.1: X-ray powder diffraction pattern of orthorhombic  $\text{Sr}_2\text{P}_2\text{O}_7$  [1].

The X-ray powder diffraction patterns of  $\text{Pr}_6\text{O}_{11}$  doped with different amounts (0.5%, 1%, 2%, 3%, 4%, 5%, 10% and 15%) were also taken. X-ray diffraction analysis demonstrated that the doped patterns were similar to those of orthorhombic  $\text{Sr}_2\text{P}_2\text{O}_7$ . It can be seen from Figure 3.2(a) that the 15% and 10%  $\text{Pr}_6\text{O}_{11}$  doping had small effects on the XRD patterns by lowering the intensities of two most intense peaks while the remaining peak positions being unchanged. Figure 3.2(a) and (b) also shows that the 5–0.5%  $\text{Pr}_6\text{O}_{11}$  doped powder patterns were very similar to those of orthorhombic  $\text{Sr}_2\text{P}_2\text{O}_7$ . It can be summarized that X-ray powder diffraction pattern

for the doped products is in fair agreement with the pattern, indicating the phase purity of the as-synthesized samples of the title compound  $\text{Sr}_2\text{P}_2\text{O}_7$ .

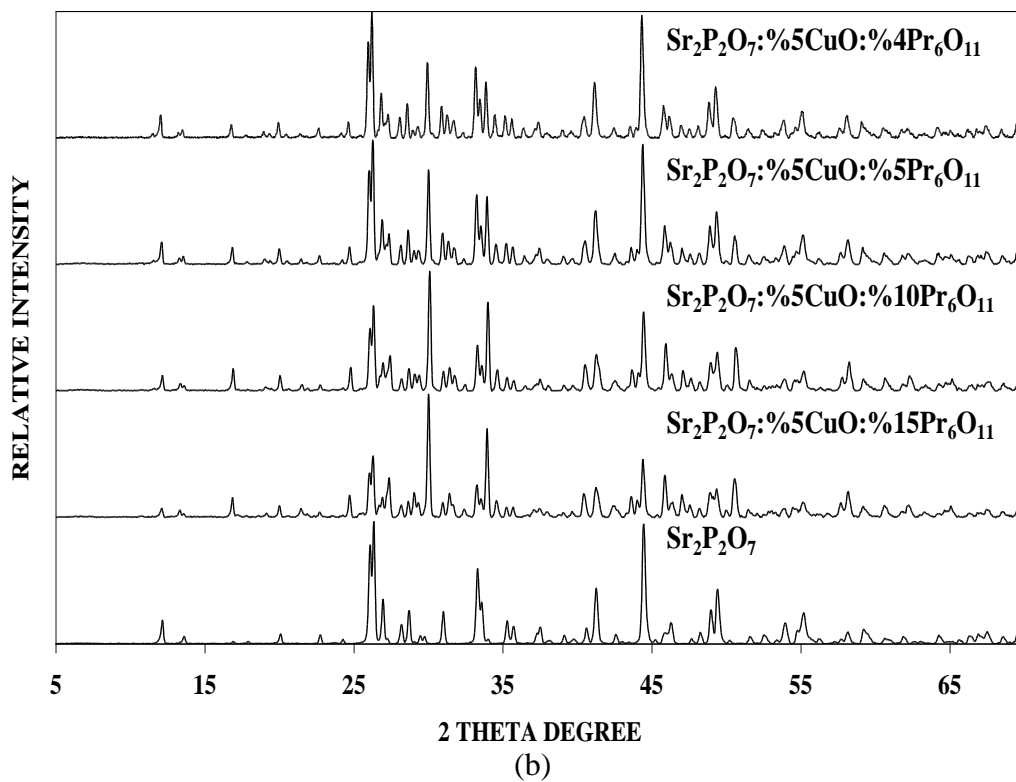
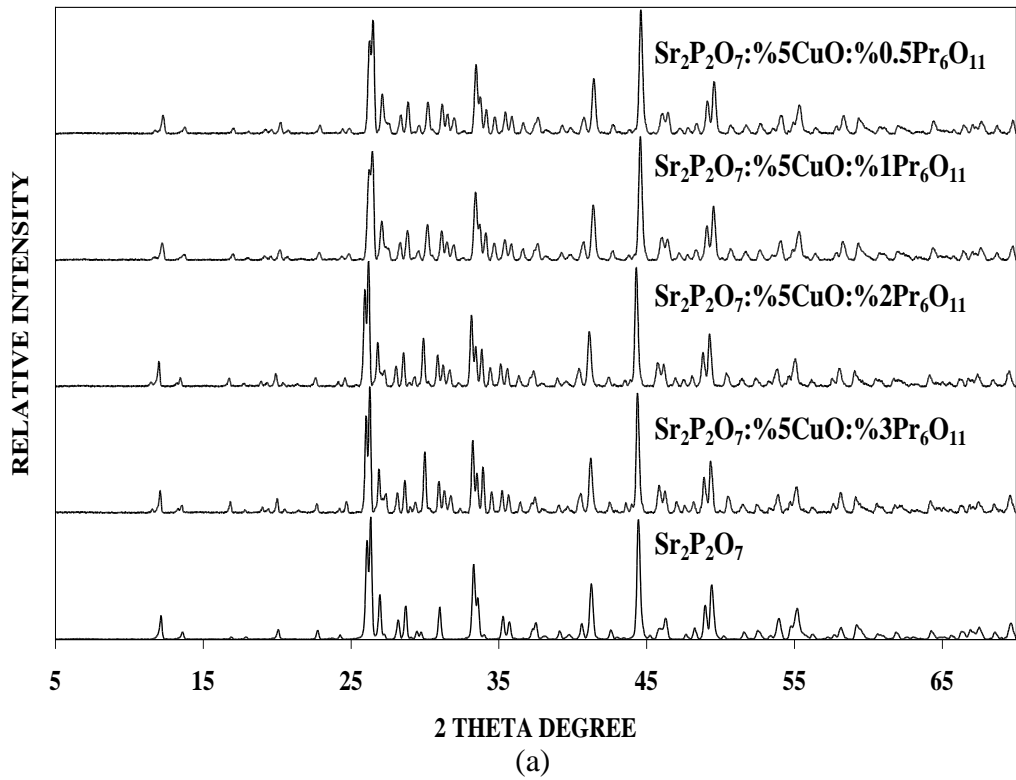


Figure 3.2: The powder X-ray diffraction patterns of 5% CuO and (a) 3%, 2%, 1%, and 0.5% Pr<sub>6</sub>O<sub>11</sub> doped  $\text{Sr}_2\text{P}_2\text{O}_7$  and (b) 15%, 10%, 5% and 4% Pr<sub>6</sub>O<sub>11</sub> doped  $\text{Sr}_2\text{P}_2\text{O}_7$  [1].

## **3.2. Equipments**

### **3.2.1. Annealing Ovens and General Heat Treatment**

Before the subsequent irradiation, the samples were first annealed to erase any residual information and then quickly cooled in air to RT. The annealing procedures were done at different temperatures with a microprocessor controlled Nuve FN 501 type electrical oven for different intervals ranging between 1 min to 24 hours. In this study, the samples were generally annealed at  $400 \pm 1$  °C for 1 hour through the experiments. The temperature is measured with a Chromel-Alumel thermocouple placed in close proximity to the samples. Temperature of the electrical oven was continuously monitored during the annealing period. The temperature sensitivity of the oven was estimated to  $\pm 1$  °C.

### **3.2.2. Radiation Source and Irradiation Procedure**

Irradiation applied on the sample about 25 °C (room temperature) with beta radiation from a calibrated  $^{90}\text{Sr}$ - $^{90}\text{Y}$  radiation device (Figure 3.3). The activity of  $\beta$ -radiation device irradiates about 100 mCi. It is calibrated by manufacturer on March, 10, 1994. The recommended working lifetime is about 15 years. Strontium-90 emits high energy beta particles from their daughter products ( $^{90}\text{Sr}$   $\beta$ -0.546 MeV together with  $^{90}\text{Y}$   $\beta$ -2.27 MeV). The irradiation equipment is an additional part of the 9010 Optical Dating System which is purchased from Little More Scientific Engineering, UK (Figure 3.3). The irradiation source equipment interfaced to a PC computer using a serial RS-232 port. The samples were irradiated for 15 minutes at room temperature with a  $^{90}\text{Sr}$ - $^{90}\text{Y}$  beta ( $\beta$ ) source delivering about 0.9 Gy/min. The samples were irradiated to various dose levels between  $\approx 0.1$  Gy and  $\approx 110$  Gy during the variable dose method. 20 mg of powder were used for each measurement. The time duration between irradiation and TL reading was always kept constant at about 1 min to eliminate the possible fading in the low temperature peak between RT and 30 °C. All experiments were performed inside a dark room in order to prevent any influence of the environment light on the glow curves.

### **3.2.3. TL Analyzer and TL Measurements**

Thermoluminescence glow curves of  $\text{Sr}_2\text{P}_2\text{O}_7:\text{Cu,Pr}$  compounds were obtained by using a Harshaw QS 3500 Manual type TL reader which has an S-11 response photomultiplier tube (Figure 3.3). The reader is interfaced to a PC where the TL signals were studied and analyzed. Glow curves were measured using a platinum planchet at a linear heating rate of  $1\text{ }^\circ\text{C s}^{-1}$  from room temperature (RT) up to  $400\text{ }^\circ\text{C}$ . For the variable heating rate method heating rates were varied from 1 to  $10^\circ\text{C/s}$ . Each measurement two times repeated, the second time is expected to be background of the first one so that the analyses have done at end of the all applications.

A standard clean glass filter was always installed in the reader between sample and photomultiplier tube. This filter allows the light whose wavelength is between  $\approx 250$  and  $\approx 1000$  nm to pass through it and thereby eliminates unwanted infrared light emitted from the heater. All functions are divided between the reader and the specialized TLD Shell software that runs on the PC. All data storage, instrument control, and operator inputs are performed on the PC. Signal acquisition and conditioning are performed in the reader. In this way, each glow curve can be analyzed using a best-fit computer program based on a Marquardt algorithm minimisation procedure, associated to first-order and general-order kinetic expressions. The program resolves the individual peaks present in the curve, giving the best values for the different peak parameters. The instrument includes a sample change drawer for inserting and removing the TLD elements. The reader uses contact heating with a closed loop feedback system that produces adjustable linearly ramped temperatures from 1 to  $50\text{ }^\circ\text{C}$  per second accurate to within  $\pm 1\text{ }^\circ\text{C}$  to  $400\text{ }^\circ\text{C}$  in the standard reader.

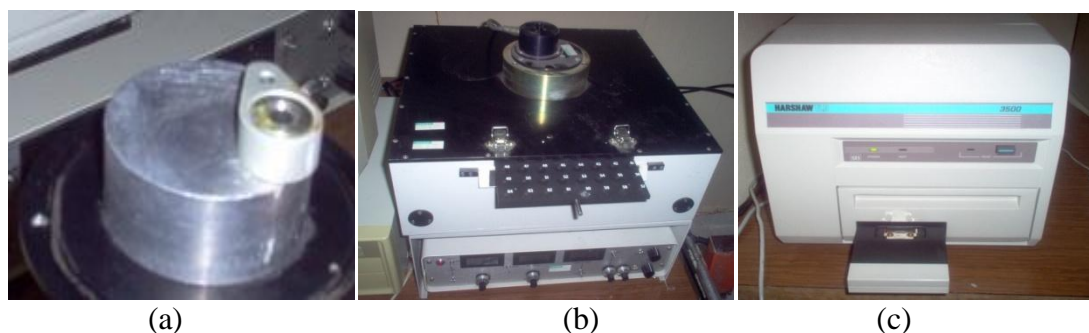


Figure 3.3 Experimental equipments (a)  $^{90}\text{Sr}$ - $^{90}\text{Y}$   $\beta$ -source (b) 9010 Optical Dating System (c) Harshaw TLD System 3500.

### 3.3 Experimental Procedure

The following procedures were employed in this study:

1. In the investigation of trapping parameters, the samples were irradiated to various dose levels by a  $^{90}\text{Sr}$ - $^{90}\text{Y}$  beta source.
2. In order to isolate glow peaks from each other, the thermal cleaning method was performed. The criterion was used to eliminate low temperature glow peaks with a minimum loss of intensity in the selected peak.
3. In the storage time experiments, the fading measurements were carried out with a group of individually calibrated samples in the following manner. After irradiation of all samples, the first of them was readout promptly, the second one was readout after 1 day and this procedure was continued with 1 day interval until reading the last sample in the group. The measurements were carried out up to 30 days. During the experimental procedure, all materials were stored in the dark about RT. All the dosimeters are of the same batch and the experimental condition was kept as similar as possible.
4. In a parallel experiment to study the influence of the heating rate, linear heating rates were chosen from 1 °C/s to 20 °C/s. The heating rates less than 1 °C/s was not applied, because it is not possible to obtain from our TL reader. On the other hand, at high heating rates there may be a considerable temperature lag between sample and planchet causing a difference between the measured and crystal temperature. Therefore, the upper limit of the heating rate was restricted by 20 °C/s.

## CHAPTER 4

### EXPERIMENTAL RESULTS and DISCUSSIONS

#### 4.1. Effect of Doping Concentration of Cu and Pr on the Glow Peaks of $\text{Sr}_2\text{P}_2\text{O}_7$

As mentioned previously, the activators such as Cu and various rare earth elements doped in  $\text{Sr}_2\text{P}_2\text{O}_7$  were previously studied by Yazıcı et al. They were observed that Pr along Cu-doped samples showed much more TL intensity than the others [1]. Therefore, the TL features of Pr and Cu-doped  $\text{Sr}_2\text{P}_2\text{O}_7$  were studied in detail in this thesis. After different amounts of Pr and 5% Cu-doping to  $\text{Sr}_2\text{P}_2\text{O}_7$  powder samples, the glow curve obtained which one is one of the glow curve elected in many of the glow curves of the sample. After the production of the samples, they annealed in an annealing oven and then irradiated with beta particles at RT to obtain the glow curves after irradiation (Figure 4.1).

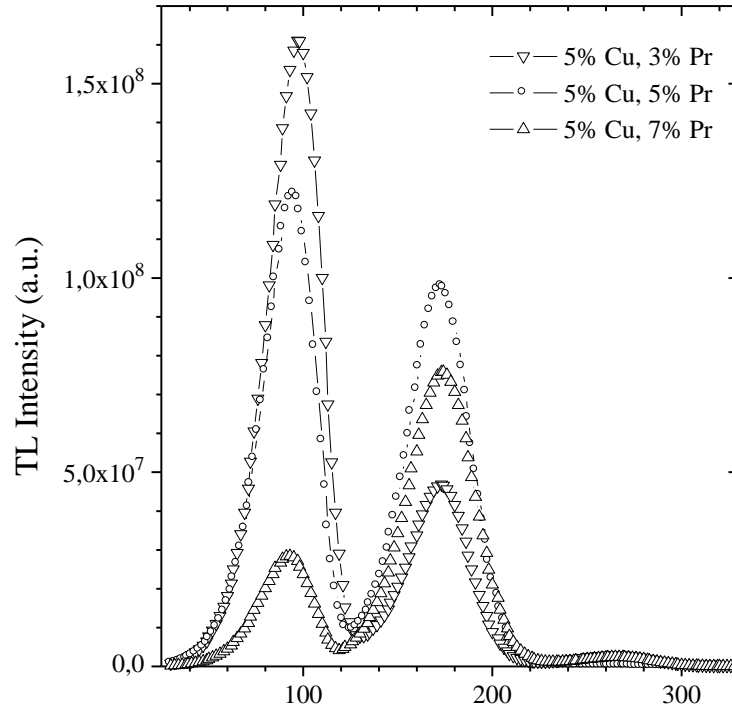


Figure 4.1: The thermoluminescence glow curves of %5 Cu and various Pr-doped  $\text{Sr}_2\text{P}_2\text{O}_7$  samples [1].

It was seen that the shape of TL glow curve structures of  $\text{Sr}_2\text{P}_2\text{O}_7$  samples remains remarkably constant after different amounts of doping with Pr and Cu. Therefore, it could be concluded that the shapes of glow curves of this sample show a concentration independent character. But, the intensities of glow peaks were only changed with the amount of doping concentration of Pr. As seen, the intensity of dosimetric glow peak at 180 °C is firstly increased with the level of Pr-concentration up to 5% and then it decreases with the addition of Pr. But, the intensity of glow peak 1 at 90 °C was continuously decreasing with increase in the level of Pr-concentration.

#### 4.2. Annealing Procedure of $\text{Sr}_2\text{P}_2\text{O}_7:\text{Cu,Pr}$

To develop the performance of TL material before the irradiation, an annealing procedure was usually utilized before the investigation of TL properties of Cu and Pr-doped  $\text{Sr}_2\text{P}_2\text{O}_7$ . Because; it was known that the heat-treatment is usually reestablished the defect equilibrium that exists in the material before the irradiation and the heating can also empty the deep traps to avoid its influence on the TL sensitivity of a given peak since they can act as competitors [1]. Because of this, one of the first problems researched in the given study is the annealing procedure to be used in order to eliminate the effects of the previous irradiations. For evaluating the

reproducibility of the dose measurements attainable using  $\text{Sr}_2\text{P}_2\text{O}_7:\text{Cu,Pr}$ , the TL stability after repeating processes of the both oven and readout annealing procedures was tested at different dose levels (1.2 Gy and 12 Gy) and the comparison of TL sensitivity of TL dosimeters after oven and readout anneal was performed. The experiment was carried out at 300 °C for 15 min and 400 °C for 15 and 30 min and then the sample was rapidly cooled to room temperature after each heat treatment.

The intensity is obtained by the integral of the peak areas of the low temperature glow peak at 80°C and dosimetric glow peak at 180 °C by the GCD program. In the readout annealing procedures without additional annealing in an oven, firstly, some samples after their background reading were irradiated to a test dose  $\approx 1.2$  Gy (or 12 Gy). The specimen is heated by constant heating rate of 1 °C/s and then glow curves of the process was recorded. Then the process is repeated after the irradiation of the sample and reading out. As observed, that the shape of the glow curves are similar for all cases after the irradiation both at  $\approx 1.2$  Gy and 12 Gy. However, as seen from Figure 4.2, the intensities of glow peaks were highly increased after repeated cycles. Particularly, when the dose levels increased, the intensities of both peak increase  $\approx 40$ -60% after 4-5 repeated cycles of irradiation-readout annealing and then they are seen as approximately stable between 40 and 60 level up to ten repeated cycles. Therefore, it was decided that an oven annealing is necessary to get a stable TL response and the lowest background. Therefore, the oven annealing procedures were firstly carried out at 300 °C for 15 min and then the sample was rapidly cooled to room temperature after each heat treatment. The obtained results represent that when the samples annealed in an oven at 300 °C for 15 min after irradiation with high doses, the intensity of peak 1 has a good stability within the less than 5% based on standard deviation over more than 10 repeated cycles. On the other hand, it was found that this annealing procedure is insufficient to completely empty the deep traps of dosimetric peak in  $\text{Sr}_2\text{P}_2\text{O}_7:\text{Cu,Pr}$  and restore the original TL sensitivity of this peak and thereupon the TL dosimeters. Therefore, another annealing procedure at 400 °C for 15 min was again adopted on the samples. But, it was observed that the similar results of annealing at 300 °C for 15 min were obtained in this case, too. Therefore, it was decided that these annealing procedures are not enough to restore the original sensitivity of TL dosimeters. On the other hand, the obtained results confirmed that an annealing at 400 °C for 30 min was only sufficient to erase the increase in the signal of dosimetric peak totally and return the



original TL sensitivity of Cu and Pr doped  $\text{Sr}_2\text{P}_2\text{O}_7$  (Figure 5.2). The results showed that the readout and oven annealing procedures at 400 °C for 30 min show a very good stability within less than 5% based on standard deviation over more than 10 repeated cycles. On the other hand, it should be mentioned that when the samples are annealed at higher temperature above 400 °C (i.e. 450 or 500 °C) before irradiation, the intensity of both the glow peaks of this sample is continuously decreased with increase in experimental cycles. Because of this, the annealing procedures above 400 °C are not convenient in this sample. As a result, it can be mentioned that during routine applications of TL detectors for dose levels less than  $\approx 12$  Gy, a readout annealing up to 400 °C appeared to be a convenient annealing procedure (Figure 4.2). Consequently, if the previous history of the material is unknown, it is advantageous to anneal the sample at 400 °C for 30 min before putting it to any dosimetric use.

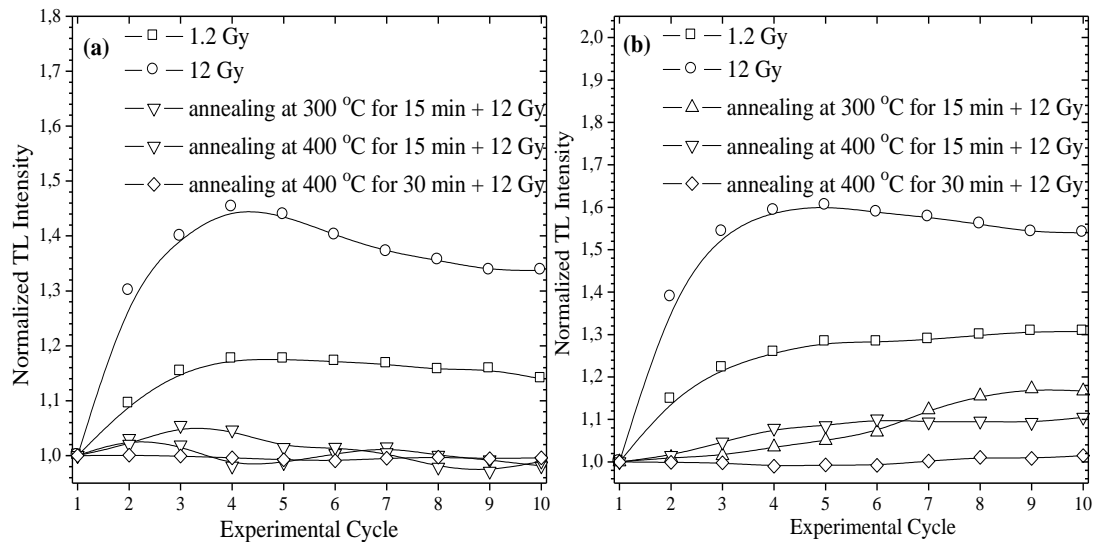


Figure 4.2: Reproducibility of deconvoluted areas of glow peaks:(a) peak 1 and (b) peak 2 of  $\text{Sr}_2\text{P}_2\text{O}_7:\text{Cu,Pr}$  through ten repeated cycles of irradiation-readout annealing.

### 4.3. The glow curve analysis of $\text{Sr}_2\text{P}_2\text{O}_7:\text{Cu,Pr}$

Previously published studies have indicated that the determination of  $E_a$  and  $s$  mainly depends on the prior knowledge of kinetic order ( $b$ ) and the exact number of glow peaks in the glow curve [11, 41-44]. The investigations were based on the principles of different properties response patterns of glow peaks for duration of irradiation. For many conditions, the glow peaks raise linearly at low-level exposure. No major distinguish in the shapes of overlapped peaks can be seen at this level. While the exposure level increases, the improve of TL peaks would activate in unlike patterns. When a few of them are linear while others are supralinear or sublinear.

That is why, the many-overlapped glow peaks happen to be noticeable through a series of high-level irradiations.

In TL theory [2, 20,21,24], the peak temperatures of glow peaks are expected to change only with heating rate for  $b = 1$ . That is why, for a constant heating rate ( $\beta$ ), the peak temperature should not be affected by other experimental parameters and must be fairly constant within the limit of experimental uncertainties. However, for  $b \neq 1$  and below the trap saturation points  $\{n_o$  (concentration of trapped electrons)  $< N_t$  (concentration of traps)}, it is usually received that the peak temperatures are shifted to the lower-temperature side with increasing dose levels. Hence, to form an opinion about the number of glow peaks and  $b$  of all individual glow peaks in the glow curve structure of  $\text{Sr}_2\text{P}_2\text{O}_7:\text{Cu,Pr}$ , the additive dose (AD) method was first utilized in the current study. To do this, the samples were irradiated at different doses to check the dose dependence effect on the peak temperature ( $T_m$ ) position of the glow peaks. This is a simple test for the first-order kinetics. Some of the selected glow curves after different dose levels are shown in Figure 4.3. The experimental observations have clearly shown that there were no significant changes in the peak temperatures of glow peaks of  $\text{Sr}_2\text{P}_2\text{O}_7:\text{Cu,Pr}$  with increasing dose level (Figure 4.3). The positions of peak temperatures of glow peaks of  $\text{Sr}_2\text{P}_2\text{O}_7:\text{Cu,Pr}$  are within the experimental error  $\pm 4$  °C for all the doses (Figure 4.4)

The recorded glow curves after the AD experiment were also used to test the possible number of glow peaks in the glow curve of  $\text{Sr}_2\text{P}_2\text{O}_7:\text{Cu,Pr}$  and their kinetic parameters by the peak shape (PS) method. This method is based on the shape and full width at half maximum ( $\text{FWHM} = T_2 - T_1$ ) of a single glow peak and the values of  $E_a$  were determined by the modified PS method of Chen [49]. According to this method, the  $b$  of a single peak is easily obtained by means of the geometric factor  $\{\mu_g = (T_2 - T_m) / (T_2 - T_1)\}$  and  $\mu_g$  changes with the order of kinetics  $b$  from  $\approx 0.42$  to  $\approx 0.52$ , where these two limits correspond to first- and second-order kinetics, respectively.

The shift in the low half-maximum temperature  $T_1$ , high half-maximum temperature  $T_2$  together with peak temperature  $T_m$ , and the change in  $\mu_g$  with exposed dose levels of dosimetric glow peak are also seen in Figure 4.5, Figure 4.6 and Figure 4.7. The experimental observations have clearly demonstrated that there were no large changes in the shapes of glow peaks of  $\text{Sr}_2\text{P}_2\text{O}_7:\text{Cu,Pr}$  with increasing dose level (Figure 4.4 and Figure 4.5). i.e. the peak temperature ( $T_m$ ) of the dosimetric

peak of  $\text{Sr}_2\text{P}_2\text{O}_7:\text{Cu,Pr}$  does not shift to lower temperatures sides as the dose increases and it becomes approximately constant around  $170\pm 2$  °C. Similarly, the peak temperature of peak 1 does not shift to lower or higher temperature sides and it becomes approximately constant around  $95\pm 1$  °C). This result indicates that both glow peaks of  $\text{Sr}_2\text{P}_2\text{O}_7:\text{Cu,Pr}$  should have first-order kinetics. When the dosimetric peak was considered to be a single peak, it was observed that  $\mu_g$  is greater than 0.42 and less than 0.52 for all exposed dose levels. In general, its value changes between 0.48 and 0.49. This means that the kinetic order of this peak is greater than first-order but less than second-order. Thus, it has a general-order kinetic and its value is on the order of  $b=1.5\pm 0.1$ .

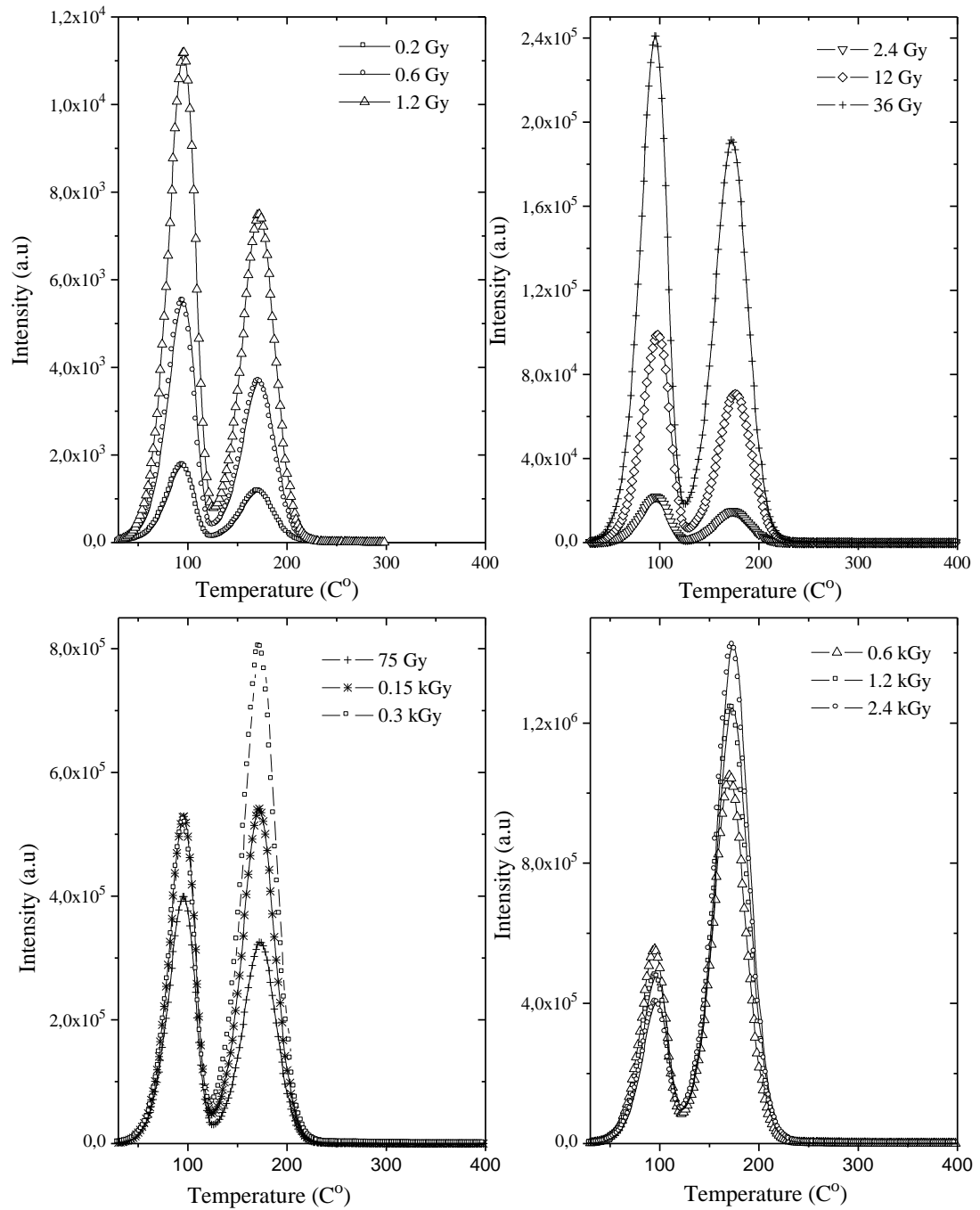


Figure 4.3: The glow curve of  $\text{Sr}_2\text{P}_2\text{O}_7:\text{Cu,Pr}$  measured after various radiation dose levels ( $\beta=1\text{ }^{\circ}\text{Cs}^{-1}$ ).

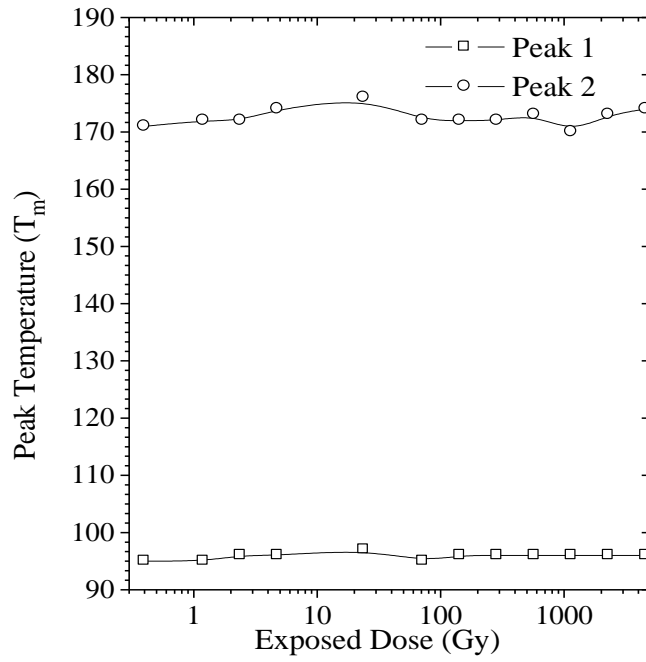


Figure 4.4: The peak temperatures  $T_m$  of glow peaks of  $Sr_2P_2O_7:Cu,Pr$  as a function of exposed dose level.

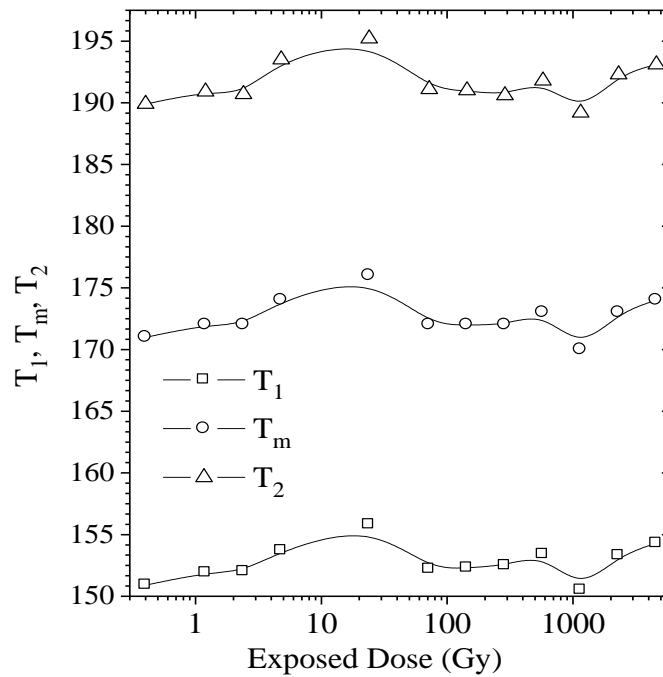


Figure 4.5: The peak temperature  $T_m$ , low half-maximum temperature  $T_1$  and high half-maximum temperature  $T_2$  of dosimetric glow peak of  $Sr_2P_2O_7:Cu,Pr$  as a function of exposed dose level.

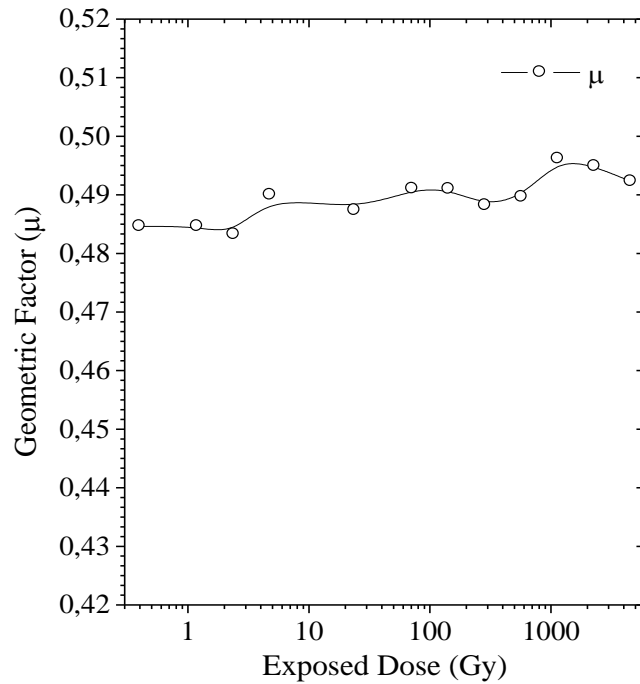


Figure 4.6: The geometric factor  $\mu_g$  of dosimetric glow peak of  $\text{Sr}_2\text{P}_2\text{O}_7:\text{Cu,Pr}$  as a function of exposed dose level.

The plots of calculated activation energies by the peak shape method are shown in Figure 4.7. Note that the dosimetric peak is assumed to have one component during the calculation of  $E_a$  by the peak shape method. As seen from Figure 4.6, when the dose level is increased, the activation energies indicated from the three shape parameters of the dosimetric glow peak show slight increase from  $1.30 \pm 0.1$  eV to  $1.35 \pm 0.1$  eV between 0.2 and 200 Gy. And then above 200 Gy, they become approximately constant around  $1.35 \pm 0.1$  eV with increasing dose levels up to the applied maximum dose ( $D \approx 5$  kGy) in the present study. This result again indicates that the dosimetric peak of this material is not a first-order glow peak but it has a general-order ( $b \neq 1$ ) glow peak.

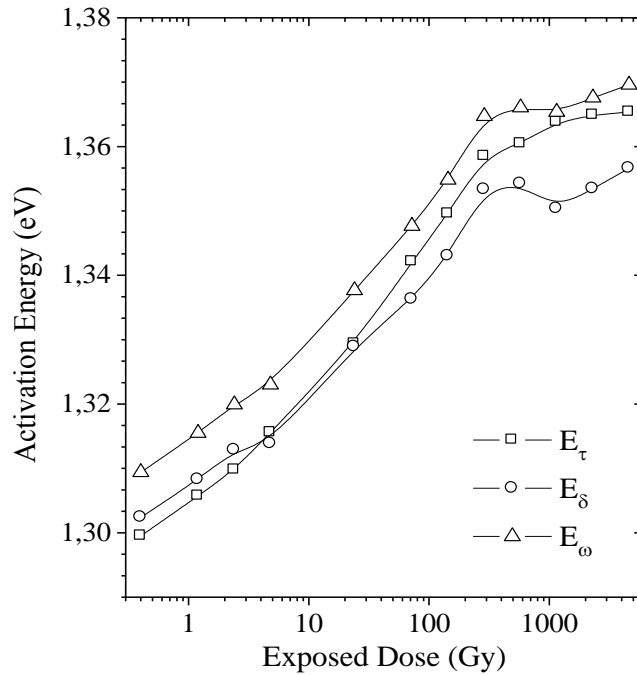


Figure 4.7: The activation energy  $E_a$  of the dosimetric glow peak of  $\text{Sr}_2\text{P}_2\text{O}_7:\text{Cu},\text{Pr}$  determined by PS method as a function of exposed dose levels ( $\beta = 1^\circ\text{C s}^{-1}$ ).

#### 4.4. Determination of Number and Position of Glow Peaks by $T_m(E_a)-T_{\text{stop}}$ Method

In an attempt to better find the number of glow peaks, peak temperatures and their related kinetic parameters, the method of repeated initial rise (RIR) was also applied to the TL glow curves of  $\text{Sr}_2\text{P}_2\text{O}_7:\text{Cu}, \text{Pr}$  in the temperature ranges from  $59^\circ\text{C}$  to  $214^\circ\text{C}$ . A strong overlapping of TL peaks makes this method the most suitable procedure for the determination of number and position of glow peaks. A plot of  $T_m$  against  $T_{\text{stop}}$  shows a stepwise curve after  $T_m-T_{\text{stop}}$  experiment and each flat region indicates the approximate position of an individual peak. A raise of  $T_m$  at the end of the flat region is an indication that the TL kinetics has an order higher than one. Peaks with first-order TL kinetics show a sharp rise to the next flat region. However, in the case of highly overlapping glow peaks, the sharp rise can be slightly smoothed out. Here, an irradiated sample is heated at a linear heating rate to a temperature  $T_{\text{stop}}$  corresponding to a point on the low temperature tail of the first peak. The sample is then cooled down quickly to room temperature and then reheated at the same rate to record all of the remaining glow curves, and the position of  $T_m$  is noted. The process is repeated several times with the same annealed/irradiated sample at some different  $T_{\text{stop}}$  values, and two measurements were taken within each

10 °C region in this study. The heating rate used was 1 °Cs<sup>-1</sup> and the exposed dose level was always set to 12 Gy. Some of the selected glow curves after  $T_m-T_{stop}$  procedure are indicated in Figure 4.8 and Figure 4.9.

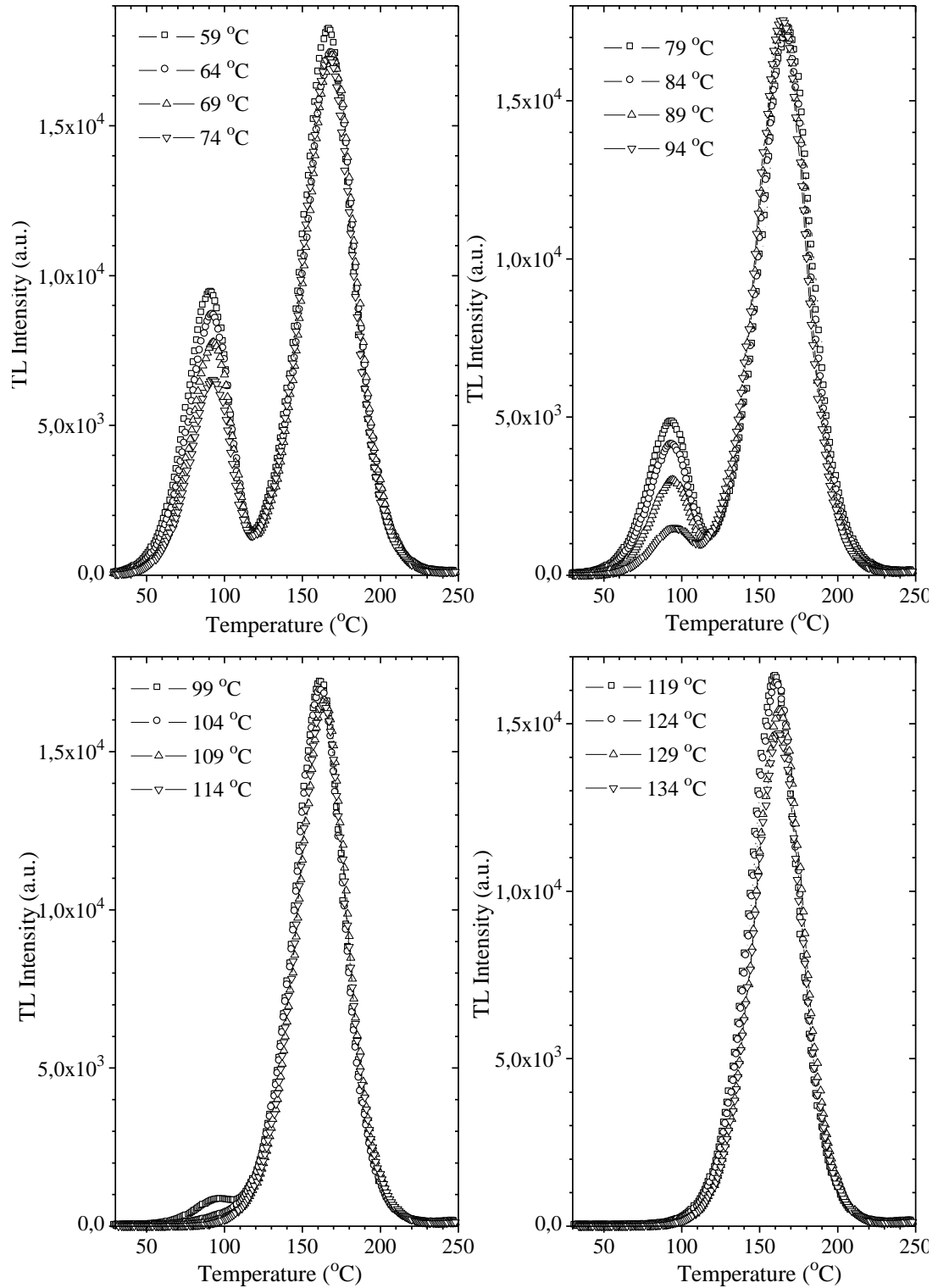


Figure 4.8: Some of the selected glow curves of Sr<sub>2</sub>P<sub>2</sub>O<sub>7</sub>:Cu,Pr after different  $T_{stop}$  temperatures between 59 °C and 134 °C at a linear heating rate  $\beta = 1$  °C s<sup>-1</sup>. The exposed dose levels are always adjusted to  $\approx 12$  Gy.



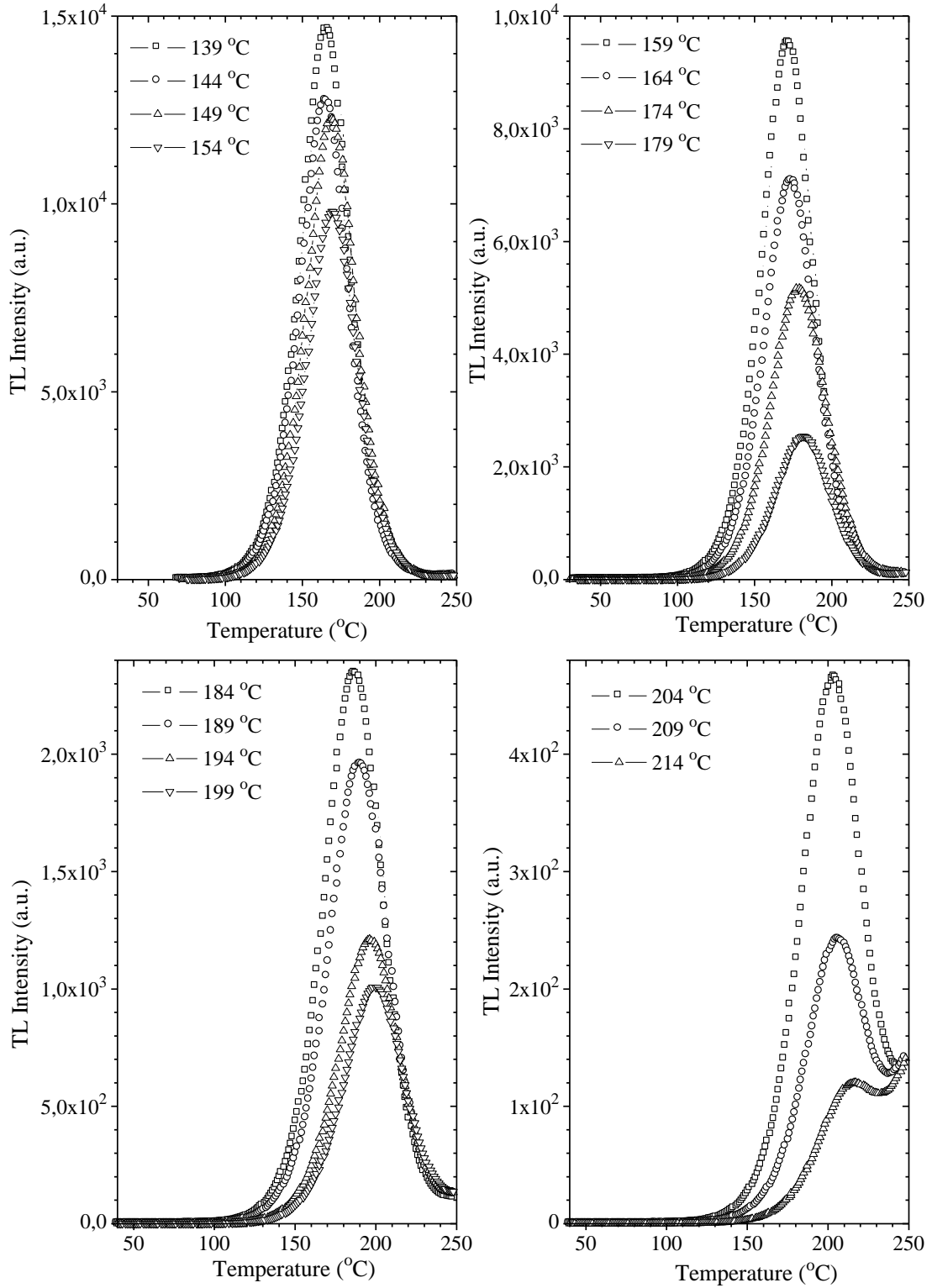


Figure 4.9: Some of the selected glow curves of  $\text{Sr}_2\text{P}_2\text{O}_7:\text{Cu,Pr}$  after different  $T_{\text{stop}}$  temperatures between  $139\text{ }^\circ\text{C}$  and  $214\text{ }^\circ\text{C}$  at a linear heating rate  $\beta = 1\text{ }^\circ\text{C s}^{-1}$ . The exposed dose levels are always adjusted to  $\approx 12\text{ Gy}$ .

A plot of the  $I_m$  versus  $T_{\text{stop}}$  curves for glow peaks (P1 and P2) of Cu and Pr-doped  $\text{Sr}_2\text{P}_2\text{O}_7$  are shown in Figure 4.10. As seen; seen there is no plateau region in

the plots of  $I_m-T_{stop}$ , but rather continuously decrease of peak intensities of both glow peaks from the beginning of the curves up to end of the of stopping temperature. But, the decrease in the slope of first peak is always faster than dosimetric peak. The dosimetric peak slowly decreases at the beginning of the plot up to  $\approx 120^\circ\text{C}$  and then a quick decrease up to  $T_{stop}=214^\circ\text{C}$  is noticeable. It is completely vanished above  $T_{stop}>220^\circ\text{C}$ .

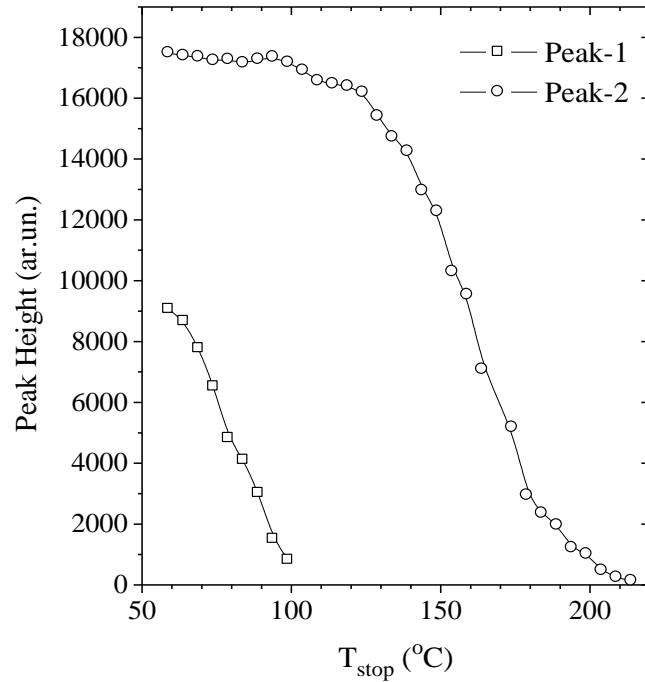


Figure 4.10:  $I_m-T_{stop}$  plot for the thermoluminescent glow peaks of  $\text{Sr}_2\text{P}_2\text{O}_7:\text{Cu,Pr}$ .

A plot of the  $T_m-T_{stop}$ ,  $T_1-T_{stop}$  and  $T_2-T_{stop}$  curves for low and high temperature glow peaks (P1 and P2) obtained with thermal cleaning method are shown in Figure 4.11. As seen; the peak temperature ( $T_m$ ), the low temperature ( $T_1$ ) at half height, and the high-temperature ( $T_2$ ) at half height of peak1 were not considerably shifted to the high temperature side with increasing  $T_{stop}$ . For example, its peak temperature ( $T_m$ ) becomes approximately constant around  $93\pm 1$ . This result indicates that this peak should have first-order kinetics. When the region of the dosimetric peak (P2) clearly checked (Figure 4.11(b)), it was again observed that there is no plateau region in the plot of  $T_m$ , but rather very slow decreases at the beginning of the plot up to  $\approx 120^\circ\text{C}$  and then a quick increase up to  $T_{stop}=214^\circ\text{C}$  is noticeable with increasing stopping temperature. A similar behavior was also observed for  $T_1$  and  $T_2$ , but the increase in the slope of  $T_1$  is especially faster than  $T_2$  above  $T_{stop}>180^\circ\text{C}$ . This situation indicates that the FWHM and half-width on the high temperature side of the peak maximum ( $\delta=T_2-T_m$ ) of the dosimetric peak of

$\text{Sr}_2\text{P}_2\text{O}_7:\text{Cu,Pr}$  are not constant, but rather change with  $T_{\text{stop}}$ . As mentioned previously, if the glow peak's maximum temperature continuously shifted to the high temperature side with increasing  $T_{\text{stop}}$ , this result indicates that TL kinetics has an order higher than one or at least it is the superposition of highly overlapped first-order glow peaks. Therefore, according to obtained result in this study by  $T_m-T_{\text{stop}}$ , the kinetic order of dosimetric glow peak must be greater than one or at least it is the combination of at least two components.

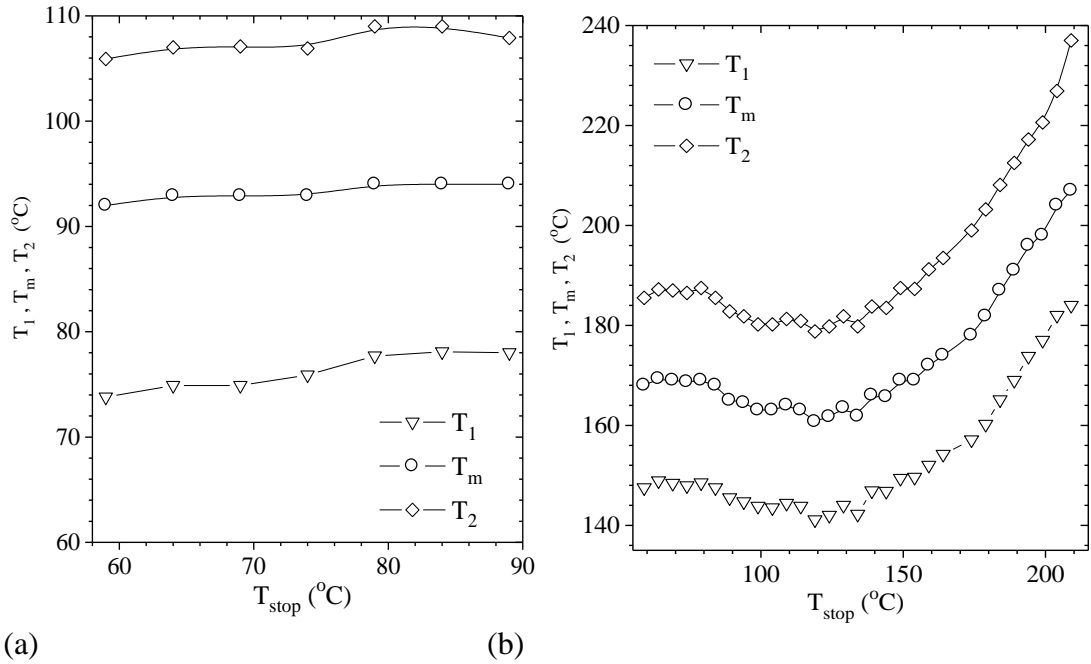


Figure 4.11:  $T_m-T_{\text{stop}}$  plot for the thermoluminescent glow peaks of  $\text{Sr}_2\text{P}_2\text{O}_7:\text{Cu,Pr}$ .

If the slopes of  $T_1$ ,  $T_m$  and  $T_2$  are different as function of stopping temperature, this situation indicates that the full width at half-maximum (FWHM) ( $\omega=T_2-T_1$ ), half width on the high temperature side of the maximum ( $\delta=T_2-T_m$ ), half width on the low-temperature side of the maximum ( $\tau=T_m-T_1$ ) of the dosimetric peak of  $\text{Sr}_2\text{P}_2\text{O}_7:\text{Cu,Pr}$  are not constant but rather change with  $T_{\text{stop}}$ . This situation is clearly shown in Figure 4.12 and Figure 4.13 for both glow peaks of Cu and Pr-doped  $\text{Sr}_2\text{P}_2\text{O}_7$ . Therefore, it was observed that the calculated values of the geometric shape factor  $\mu_g=\delta/\omega$  of both peaks always changes with increasing  $T_{\text{stop}}$  up to 214 °C. As seen, the  $\mu_g$  values of peak 1 increases from  $0.43\pm 0.01$  to  $0.48\pm 0.01$  with increasing  $T_{\text{stop}}$  up to 85 °C above that point it decreases to  $0.46\pm 0.01$  up to 90 °C (Figure 4.12(a)). On the other hand, the  $\mu_g$  values of dosimetric peak slowly increases from  $0.46\pm 0.01$  to  $0.48\pm 0.01$  with increasing  $T_{\text{stop}}$  up to 180 °C and then it

quickly increases to  $0.56 \pm 0.01$  up to  $214 \text{ }^\circ\text{C}$  (Figure 4.13(a)). The process of thermal quenching of luminescence might be one of the causes of the change in  $\mu_g$  value depending on the value of  $T_{\text{stop}}$ , since the process of thermal quenching affects the form of the glow curve due to its non-linear dependence on temperature. Another reason might be that the both peaks have general-order glow peaks and the number of empty traps increases with increasing stopping temperature, then, this could effect the  $\mu_g$  values of both peaks.

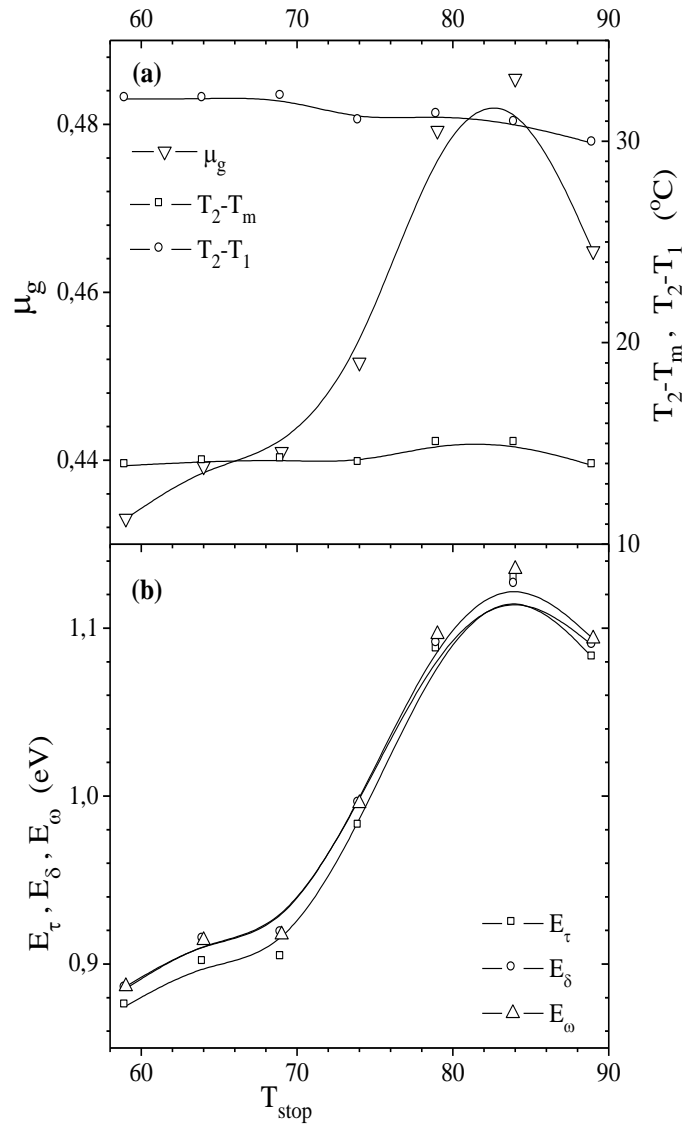


Figure 4.12: (a) The geometric factor  $\mu_g$ ,  $T_2 - T_1$  and  $T_2 - T_m$  of low temperature glow peak of  $\text{Sr}_2\text{P}_2\text{O}_7:\text{Cu,Pr}$  as a result of  $T_{\text{stop}}$  determined from the  $T_m - T_{\text{stop}}$  procedure. Lines are fits to guide the eye. (b) The activation energy ( $E_a$ ) resulting from the PS method after the  $T_m - T_{\text{stop}}$  procedure.

The recorded glow curves of Cu and Pr-doped  $\text{Sr}_2\text{P}_2\text{O}_7$  after the  $T_m - T_{\text{stop}}$  experiment were also used to indicate the activation energy of both glow peaks by

the peak shape (PS) method. The plots of calculated activation energies of both glow peaks by the PS method are shown in Figure 4.12(b) and Figure 4.13(b). Note that the both peaks were always assumed to be a single peak during the calculation of  $E_a$  in this experiment. It was observed that the calculated values of the activation energies of both peaks always changes with increasing stopping temperatures. For example, the  $E_\tau$ ,  $E_\delta$  and  $E_\omega$  values of dosimetric peak irregularly increases from  $1.2\pm 0.05$  eV to  $1.3\pm 0.05$  with increasing  $T_{\text{stop}}$  up to  $180^\circ\text{C}$  and then it quickly increases to  $1.4\pm 0.05$  up to  $214^\circ\text{C}$  (Figure 4.13(b)).

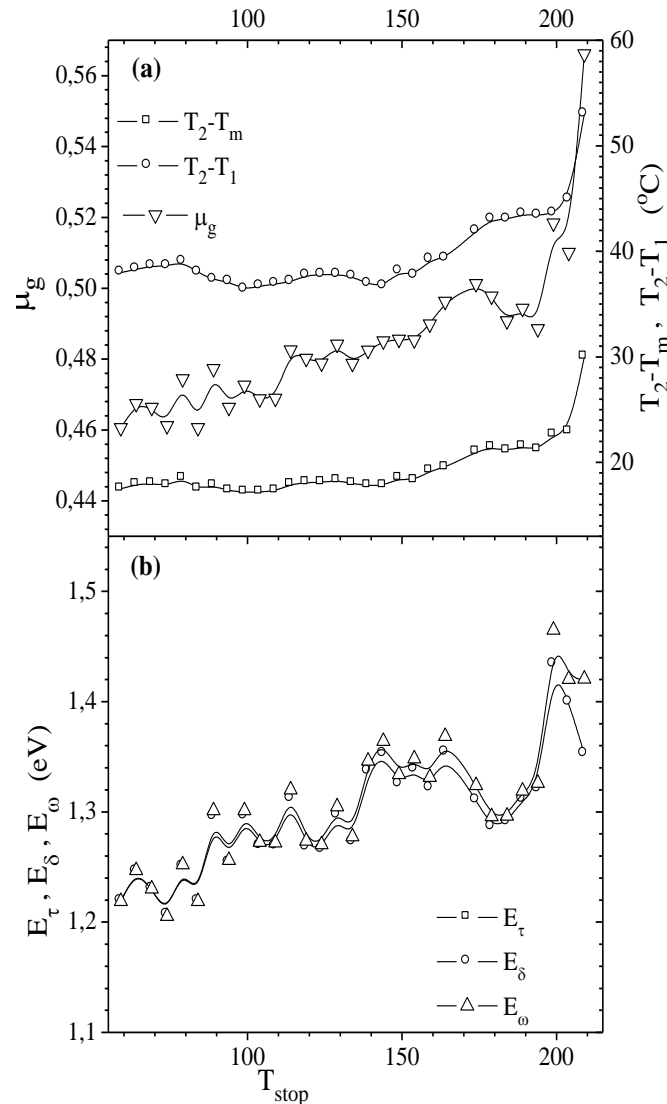


Figure 4.13: (a) The geometric factor  $\mu_g$ ,  $T_2 - T_1$  and  $T_2 - T_m$  of high temperature dosimetric glow peak of  $\text{Sr}_2\text{P}_2\text{O}_7:\text{Cu,Pr}$  as a result of  $T_{\text{stop}}$  determined from the  $T_m - T_{\text{stop}}$  procedure. Lines are fits to guide the eye. (b) The activation energy ( $E_a$ ) resulting from the PS method after the  $T_m - T_{\text{stop}}$  procedure.

In some cases, if the glow curve structure has highly overlapping glow peaks, the number of glow peaks might be better figured out with a plot of  $E_a$  against  $T_{\text{stop}}$

instead of from the  $T_m-T_{\text{stop}}$  plot. Therefore, the IR method was also employed to obtain the  $E_a-T_{\text{stop}}$  plot in this study. This method is one of the most reliable methods for evaluating  $E_a$  of a single glow peak. In this method, at the beginning of the TL glow peak, the concentration of trapped electrons  $n_0$  changes by only a small amount with temperature and thus it can be regarded as constant, so that the first- and general-order TL equations are simplified as  $I(T) \propto A \exp(-E_a/kT)$ , where  $A$  is a constant and the TL intensity is independent of  $b$ . Therefore, a plot of  $\ln(I)$  versus  $1/T$  would yield a straight line with a slope of  $-E_a/kT$ , from which  $E_a$  can readily be calculated. This method can be used only in the initial region of the TL signal up to  $\approx 10\%$  of its peak maximum ( $I_m$ ). However, if the intensity at the beginning of each peak is very low and especially when the glow curve is composed of several glow peaks, the obtained values of  $E_a$  may not reflect the actual values. Hence, in such a case, the values of  $E_a$  obtained by the IR method often need corrections. Christodoulides [80] and Singh *et al* [81] have suggested the use of high level of glow peaks to reduce the inaccuracies in  $E_a$  due to high levels of the used signal, which was also utilized in this work. Another issue during the evaluation of  $E_a$  by IR is the effect of thermal quenching effect on the evaluated  $E_a$ . This effect underestimates the values of  $E_a$  obtained by the IR method. Since the experimental glow curve shape is highly distributed by the thermal quenching effect, it cannot give reliable information about the values of  $E_a$ . However, the IR method analyses only the leading part of the glow peak and as such yields data appropriate to only that component of the TL signal comprising the full peak. Therefore, even if the IR method gives erroneous values of  $E_a$  when thermal quenching is present in the material, it should be expected that the plot of  $E_a$  against  $T_{\text{stop}}$  still gives plateau regions with a gradual decrease at the end of each plateau after the  $T_m-T_{\text{stop}}$  procedure even if the glow curve is the superposition of overlapping glow peaks.

It is well known that the thermal quenching effect is dominant in many TL dosimetric materials, i.e., in  $\text{Al}_2\text{O}_3:\text{C}$  (TLD-600) [82], in quartz [65,83], in  $\text{CaF}_2:\text{Mn}$  [84]. If the materials suffer from thermal quenching effect, the reduction of  $E_a$  values was clearly observed by previous researches in this field [85]. The result of calculated activation energies by repeated initial rise (RIR) method is shown in Figure 4.14 as a function of  $T_{\text{stop}}$ . As seen from this figure, the values of  $E_a$  become nearly constant around  $1.04 \pm 0.02$  eV, which gives the  $E_a$  value of the first glow peak (P1) up to  $T_{\text{stop}} \approx 110$  °C. Beyond this temperature ( $T_{\text{stop}} > 110$  °C), the values of  $E_a$

quickly increases and it becomes again nearly constant around  $1.26 \pm 0.04$  eV, which gives the  $E_a$  value of the dosimetric glow peak (P2) up to  $T_{\text{stop}} \approx 214$  °C. However, when it is carefully checked, it is seen that the calculated values of the activation energies in region of dosimetric glow peak (peak-2) ( $130$  °C  $< T_{\text{stop}} < 214$  °C) were continuously decreased from 1.30 eV to 1.22 eV. This means that no noticeable good flat regions were obtained after  $T_{\text{stop}} > 130$  °C. Hence, we can say that the process of thermal quenching should be effectively revealed in this sample when  $T_{\text{stop}}$  exceeds 130 °C.

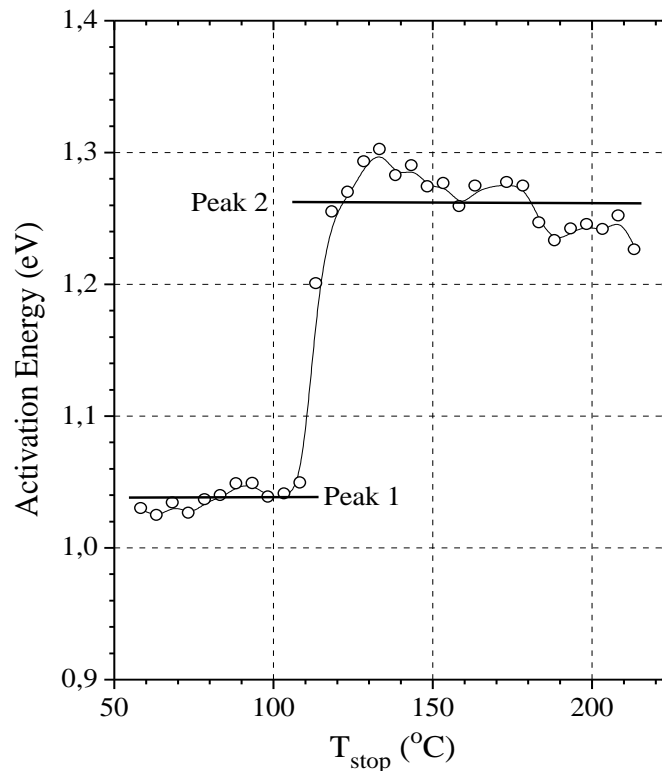


Figure 4.14: The activation energy ( $E_a$ ) resulting from the RIR method after  $T_m - T_{\text{stop}}$  procedure.

#### 4.5. Glow Curves Analysis by CGCD Method

The all glow curves were also analyzed by CGCD method to obtain the number of glow peaks. This method has become very popular to obtain the number of glow peaks in the complex glow curves and their kinetic parameters for the last four decades [47]. It is apparent that if the number of data points used in the analysis increases, the potential for accurate evaluation of number of glow peaks and their kinetic parameters gets better. Therefore, this method has great advantages over methods. However, it must be noted that different models, approximations and minimization procedures are used for the glow curve analysis in the CGCD program.

As a consequence, one may wonder whether the results of CGCD method reflect the accurate kinetic parameters of the TL peaks. According to many experienced researchers, the results obtained by the CGCD method, in some cases, seem to be unreliable. Especially, the advantages of the CGCD method may be undermined in complex TL glow curves. As a result, many possible sets of kinetic parameters could be assigned to the same glow curve if different number of glow peaks was used in the CGCD program. Therefore, the number of glow peaks was only investigated by the CGCD method in the given study. The used CGCD program, which is based on the least square minimization procedure, was developed at the Reactor Institute at Delft, The Netherlands [86]. In this study, the first-order kinetic was approximated for all CGCD evaluations by the expression 2.29 and 2.36 [86, 63].

The goodness of fit for all the measured glow curves was tested using the figure of merit (FOM) [75]. From many experiences, it can be said that, if the values of the FOM are between 0.0% and 2.5% the fit is good, between 2.5% and 3.5% is a fair fit, and  $>3.5\%$  is a bad fit. Detailed information on the deconvolution method has been given elsewhere [63].

The number of glow peaks is not a free fitting parameter during the deconvolution of the measured glow curve into individual components in the CGCD programs. If the number of peaks is not known, it can be found by fitting the glow curve several times with a different number of components up to obtaining best-fit result. Therefore, the real number of glow peaks to be in the glow curve of  $\text{Sr}_2\text{P}_2\text{O}_7:\text{Cu,Pr}$  was investigated by using different number of glow peaks in the CGCD program. In the given study, it was observed that it is not possible to fit the glow curve of  $\text{Sr}_2\text{P}_2\text{O}_7:\text{Cu,Pr}$  by two components (glow peaks) with first-order kinetics. In this case, there were large differences between experimental and computed glow curves when two first-order components were assumed in the CGCD program. However, the goodness of fit was relatively improved if the glow curves of this sample was fitted by one first and one general-order components. In this study, after many tries with different number of glow peaks, it was observed that the glow curve structure of  $\text{Sr}_2\text{P}_2\text{O}_7:\text{Cu,Pr}$  is well described by a linear combination of at least two general-order glow peaks. In this case, a reasonably good fit was always obtained. Therefore, the glow curve of  $\text{Sr}_2\text{P}_2\text{O}_7:\text{Cu,Pr}$  was always fitted with two general-order components. All of the glow curves of  $\text{Sr}_2\text{P}_2\text{O}_7:\text{Cu,Pr}$  recorded after  $T_m-T_{stop}$  experiments were analyzed by CGCD method with two general-order



kinetics. Some of them are shown in Figure 4.15 along with their components. The obtained kinetic parameters (activation energy ( $E_a$ ), frequency factor ( $\ln(s)$ ), kinetic-order (b)) along with peak intensities ( $I_m$ ) of both glow peaks are shown in Figure 4.16.

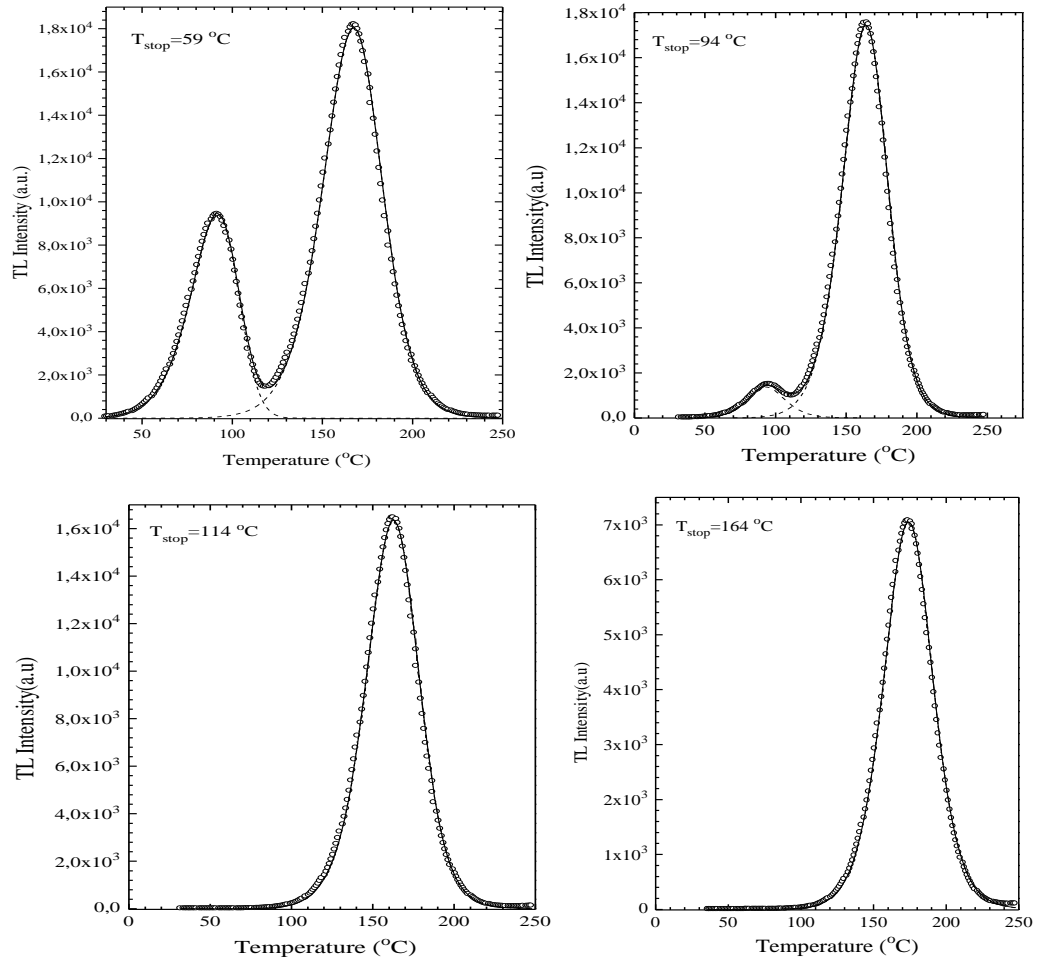


Figure 4.15: Some of the CGCD analyzed glow curves after different  $T_m-T_{stop}$  experiments ( $D \approx 12$  Gy). In all figures, open circles, solid lines and dotted lines represent the experimental points, global fitting and fitted individual peaks, respectively ( $\beta = 1^\circ\text{C s}^{-1}$ ).

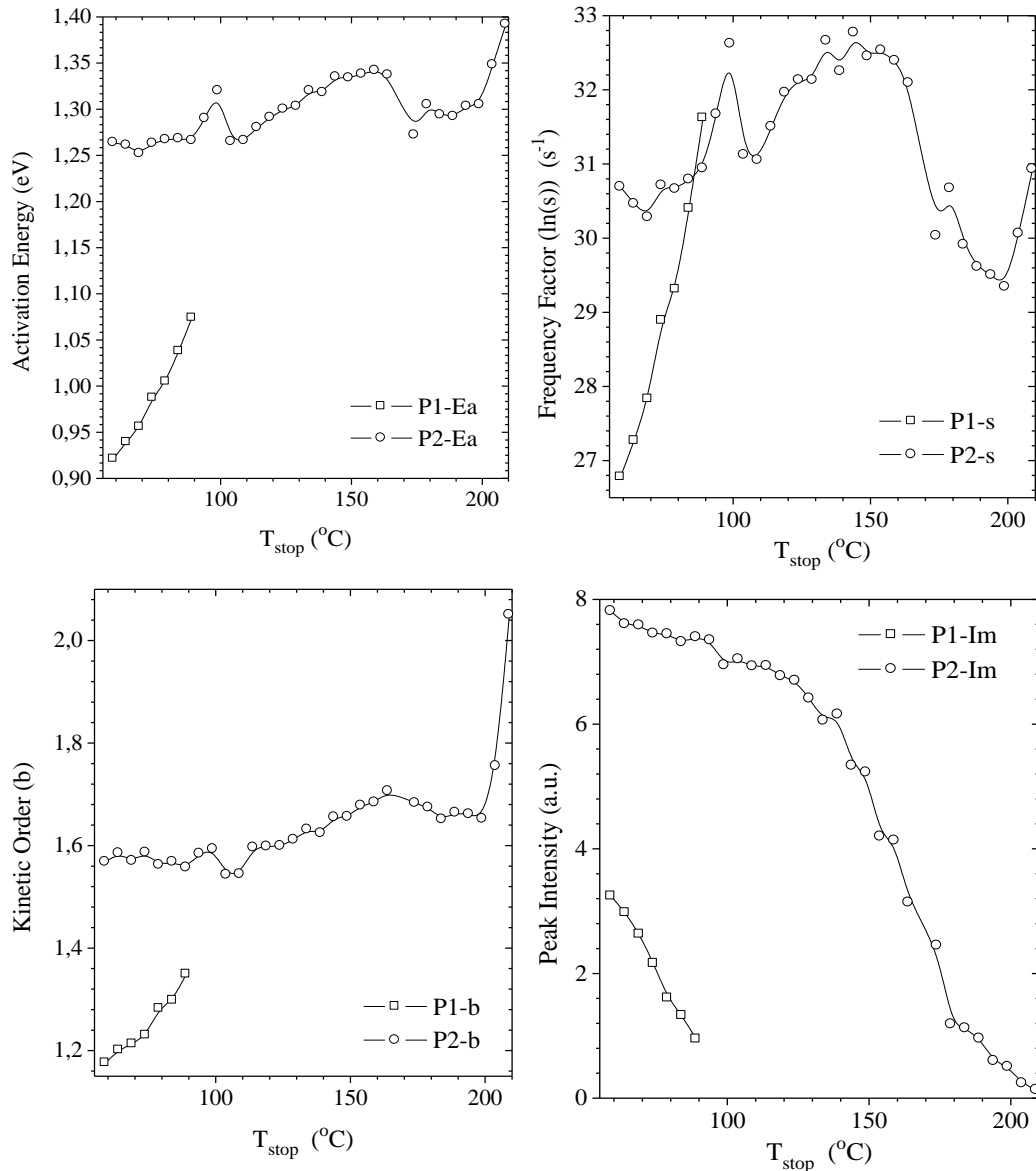


Figure 4.16: The kinetic parameters ( $E_a$ ,  $s$ ,  $b$ ) and peak intensities ( $I_m$ ) of glow peaks of  $\text{Sr}_2\text{P}_2\text{O}_7:\text{Cu,Pr}$  resulting from the CGCD method after  $T_m-T_{\text{stop}}$  procedure.

#### 4.6. The Influence of Heating Rate

In the present study, the influence of heating rates between 1 and 30 °C s<sup>-1</sup> on the peak temperatures and peak intensities of glow peaks of Cu and Pr-doped  $\text{Sr}_2\text{P}_2\text{O}_7$  was also investigated by the peak height technique. A set of glow curves measured with different heating rates is shown in Figure 4.17(a). The influence of heating rate on the glow peaks is clearly seen in this figure. As expected in theory, the peak temperatures of both glow peaks in the glow curves of  $\text{Sr}_2\text{P}_2\text{O}_7:\text{Cu,Pr}$  are shifted to higher side as the heating rate increases (Figure 4.17(b)). But the rate of shifting is decreased with increasing heating rate. On the other hand, both peak intensities of both glow peaks continuously decrease with increasing heating rate in

the investigated heating rate region. The results of the peak height of both glow peak of Cu and Pr doped  $\text{Sr}_2\text{P}_2\text{O}_7$  are shown in Figure 4.17(b). As seen, the influence of heating rates on the intensities of glow peaks is approximately equal to each other and is very effective with increasing heating rate. Figure 4.17(b) shows that the decrease in the peak height of both peaks with heating rates from 1 to 30  $^\circ\text{C/s}$  is on the order of 80%.

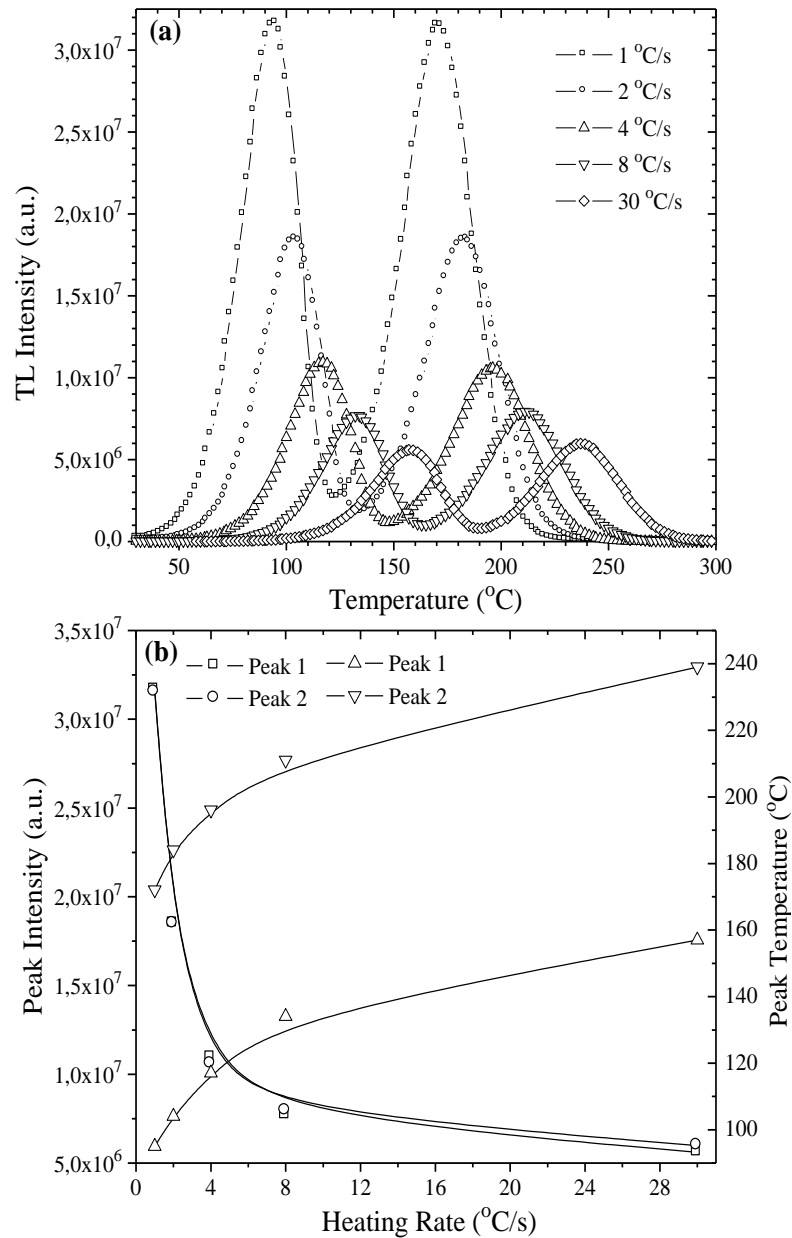


Figure 4.17: (a) Some of the selected glow curves of  $\text{Sr}_2\text{P}_2\text{O}_7:\text{Cu,Pr}$  measured at various heating rates from  $1^\circ\text{C/s}^{-1}$  to  $30^\circ\text{C/s}^{-1}$ . All the glow curves were measured after  $\beta$ -irradiation to a dose level of  $\approx 12$  Gy. (b) The peak temperatures ( $T_m$ ) and thermoluminescence response ( $I_m$ ) of glow peaks of  $\text{Sr}_2\text{P}_2\text{O}_7:\text{Cu,Pr}$  as a function of heating rate [1].

Two mechanisms have been suggested in the literature to explain the decrease in the luminescence efficiency, and both give rise to an expression of the form of

$$\eta = (1 + C \exp(-W / kT))^{-1}$$

where  $W$  and  $C$  are the quenching parameters. In the former, the reduction in intensity of TL peaks can be attributed to the thermal quenching effect. The thermal quenching of luminescence was first observed in natural quartz [43]. It was understood to be due to the increased probability of non-radiative transitions competing with radiative transitions. In fact, the luminescence efficiency of a phosphor is given by  $\eta = P_r / (P_r + P_{nr})$ , where  $P_r$  is the probability of luminescence transitions, temperature independent and  $P_{nr}$  is the probability of non-radiative transitions, which is temperature dependent. Since the increase in the heating rate resulted in an increase in the temperature of the TL glow peak, this shift in temperature was held responsible for the increase in the contribution of non-radiative transitions. Then, it was inferred that the glow peaks occurring at higher temperatures must exhibit higher thermal quenching than those occurring at lower temperatures any TLD material. Apart from the increased probability of non-radiative transitions at higher temperatures, the observed effects have also been assigned to the effects of heating rate on the migration of charge carriers released during the TL readout. If the lattice parameters are responsible for the non-radiative transitions, the raise in the moving of the charge carriers with temperature would reduce the luminescence efficiency and therefore the response will reduce at a faster heating rate. However, in order to have a tenable explanation for the variation of peak intensities with the heating rate, it will require a more detailed investigation because a single model may not be sufficient to explain the observed variations and many models can play a role in the variations of TL response of this material.

#### **4.7. Fading Studies at Room Temperature**

For used dosimeters, the emitted light due to trapping of electron must be stable to get correct result in geology and archaeology dating. For a sample to be useful in dosimetry, the TL intensity of its dosimetric peaks should be stable and not fade upon storage after exposure. Any noticeable radiation captured at room temperature will cancel the relation between TL emission and the radiation exposure that might have been liberated long time before readout. The extent of TL signal decay

over long periods is difficult if not impossible to measure directly, particularly in archaeological applications.

For researching the fading properties of glow curves in  $\text{Sr}_2\text{P}_2\text{O}_7:\text{Cu,Pr}$ , the samples were stored about the room temperature between 25 and 30 °C over a period of 1 month after beta-ray exposure. The initial analysis is done by using of CGCD method, due to planning of storage glow curves. The normalized relative results of analyzed glow curves by CGCD method are demonstrated in Figure 4.18. Each point in the figure is the average of four readings. The results demonstrated a very high decrease of the TL response during the elapsed period of time in both peaks. As seen from this figure, peak1 is quickly decreased and the fading of this peak is higher than 90% for 1 week. It was completely removed from the glow curves after the storage at room temperature for 20 days after the irradiation. So, the influence of this peak in dosimetric measurements can be easily eliminated by making the TL measurements by incorporating a pre-read anneal at about 80 °C for a few seconds in the TL reader system. On the other hand, the TL yield of dosimetric peak (peak 2) was reduced to typically 20% of its original value after 1 month storage at room temperature.

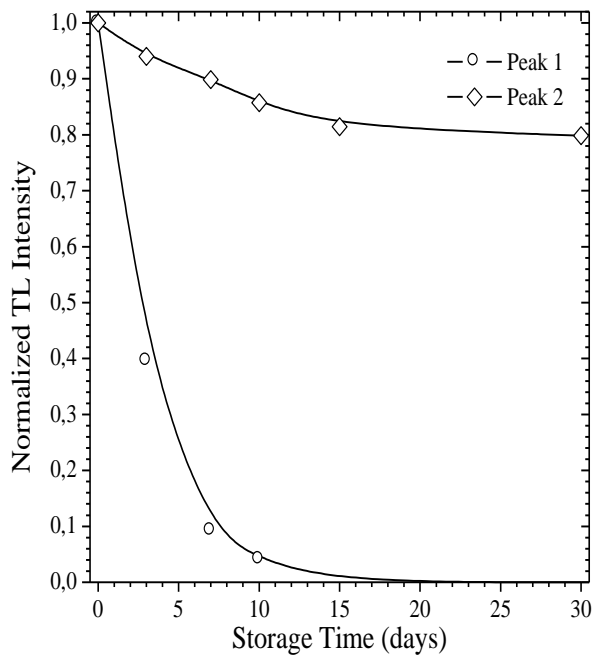


Figure 4.18: Fading evaluation of the deconvoluted peaks of  $\text{Sr}_2\text{P}_2\text{O}_7:\text{Cu,Pr}$  at room temperature in the isolated room.

The activation energies of both glow peaks of  $\text{Sr}_2\text{P}_2\text{O}_7:\text{Cu,Pr}$  were also determined by variable heating rate method. As mentioned previously, this method is based on the shift position of the temperature at the maximum ( $T_m$ ) to higher

temperatures when the heating rate is increased. However, a difficulty arises in the case of highly overlapping glow peaks when applied this method, since, then, the apparent maxima of the measured glow curve may not coincide with the actual peak maxima of the individual glow peaks. In this situation, the determined kinetic parameters by the VHR method may not reflect the real values if the glow peaks. To overcome this problem, in some cases, the thermal cleaning method was first used to clean the low temperature peaks with a minimum loss in the intensity of the main peak in question and separate glow peaks from each other. However, if the glow curve of  $\text{Sr}_2\text{P}_2\text{O}_7:\text{Cu},\text{Pr}$  was carefully checked, it was seen that the peak maxima of both glow peaks (P1 and P2) are easily distinguishable from each other. Thus, the activation energies of these peaks were calculated by the VHR method after determination of their peak temperatures by choosing their directly read maxima from the glow curves. A plot of  $\ln(T_m^2/\beta)$  versus  $(1/T_m)$  of glow peaks is shown in Figure 4.19(a-b). The calculated values of activation energies of both peaks from the slopes of these curves are also given within the inset of figure. However, it is seen that the results obtained by the VHR method are highly different from the obtained values by other methods such as PS and CGCD. The temperature lag between the heating element and the thermoluminescent sample during the TL readout in readers using contact heating is an important parameter that affects the kinetic parameters obtained by the VHR method. Therefore, it has to be taken into consideration to avoid large errors in the kinetic parameter determination by the VHR method.

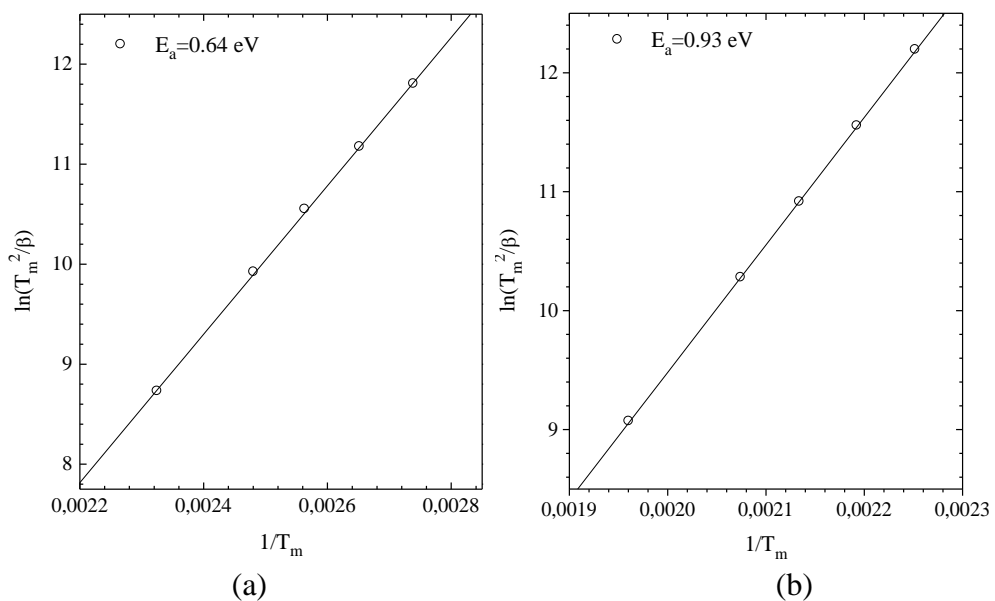


Figure 4.19: Variable heating rate plots of  $\ln(T_m^2/\beta)$  against  $(1/T_m)$  of glow peaks. (a) Peak 1, (b) peak 2.

#### 4.8. Dose Response

Another important feature of glow curves is their dependence on the excitation dose. The dose can be defined as the accumulated amount of irradiation incident on the sample during the excitation period at low temperature, or the total amount absorbed prior to the heating. In the applications in dosimetry and archaeological dating of ceramic samples, a linear dependence on the dose in broad ranges is highly desirable, but this is by no means always found to be in case. Typically, at high doses, the dose dependence curve approaches some saturation value. At low doses, linear dose dependence is quite prevalent, however super linear (or supralinear) dependence as of the lowest doses sometimes occurs. Therefore, in dosimetric investigations), it has to be considered the dose response curve of material.

The dose response of  $\text{Sr}_2\text{P}_2\text{O}_7:\text{Cu},\text{Pr}$  was studied as a function of irradiation time between 1 s ( $\approx 0.04$  Gy) and 32 hr ( $\approx 4.6$  kGy) using  $\beta$ -rays. Some of the selected glow curves after different dose levels are shown in Figure 4.3 and 4.4. Samples were annealed at 400 °C for 30 min before each use and then read immediately after irradiation. All recorded glow curves were analyzed by CGCD program and the resulting dose response curve is shown in Figure 4.20. As shown all data in dose response are plotted on a log-log scale. It is clearly seen that the obtained dose responses of both glow peaks follow similar pattern up to  $\approx 50$  Gy. As seen, it looks as that the peak areas of both peaks were linearly increased with increasing beta-ray dose up to  $\approx 50$  Gy and then a saturation effects start to appear up to applied maximum dose in the present study. Above this level ( $D > 50$  Gy), they have slightly different slopes and they are saturated at different dose levels. The calculated values of slopes of both peaks between 0.4 Gy and 50 Gy are approximately equal to each other which are equal to  $\approx 1.04$  on the log-log scale.

So, as similar to the most common TL materials,  $\text{Sr}_2\text{P}_2\text{O}_7:\text{Cu},\text{Pr}$  compound shows extremely useful TL feature of perfect linearity in its TL response obtained by peak area method with dose up to  $\approx 50$  Gy. Generally supralinearity is a characteristic of a large variety of TL materials, so TL linearity in the high dose region, over 10 Gy, is exceptionally rare. Therefore, the presented results in this work suggest that the second peak at  $\approx 180$  °C can be safely used as a dosimetric peak in medical applications and thereupon it is called as dosimetric peak in this study.

The usable dose range of many phosphors is limited at the lower end of doses by the variability in the background signal from the undosed samples. In the given study, the experimentally determined minimum detectable dose defined as that dose which gives three times the standard deviation of the zero reading of the Cu and Pr-doped  $\text{Sr}_2\text{P}_2\text{O}_7$  phosphors, is also estimated and it is found to be approximately 400  $\mu\text{Gy}$ .

The TL sensitivity of this material was also compared with the well known dosimeter TLD-100. They were given a test beta-dose of 2.4 Gy and their sensitivities were compared. As mentioned previously, the second peak at 170 °C is the most intense of glow peaks in Cu and Pr-doped  $\text{Sr}_2\text{P}_2\text{O}_7$  and hence it is important for dosimetric studies. Therefore, after the normalization to the same mass of all samples, the TL intensity of peak 2 of  $\text{Sr}_2\text{P}_2\text{O}_7:\text{Cu,Pr}$  sample was compared with intensity of peak 5 in TLD-100 and it was found that the TL intensity is approximately  $5 \pm 0.1$  of TLD-100.

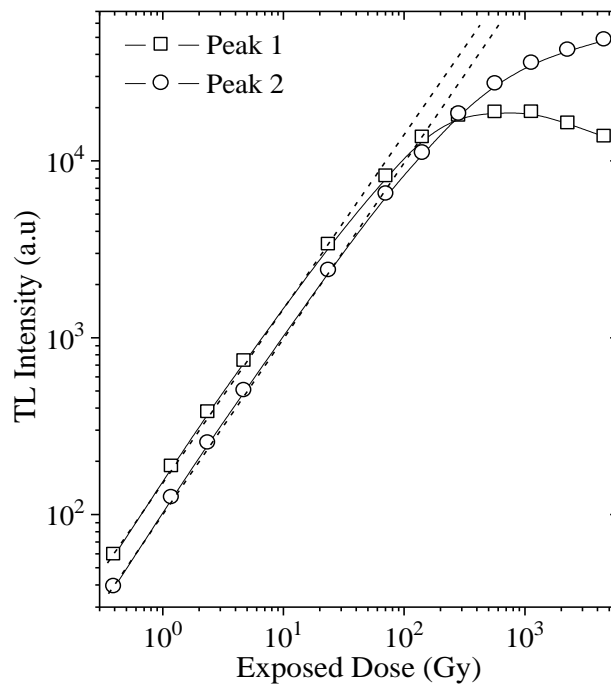


Figure 4.20: The TL dose response curve of glow peaks of  $\text{Sr}_2\text{P}_2\text{O}_7:\text{Cu,Pr}$  sample determined by the peak area of glow peaks.



## CHAPTER 5

### CONCLUSION

In the previous studies [1, 79], the thermoluminescence features of rare earth oxides (i.e. Pr<sub>6</sub>O<sub>11</sub>) along CuO doped into the previously prepared pure Sr<sub>2</sub>P<sub>2</sub>O<sub>7</sub> were studied in detail. XRD studies showed that doping did not affect the host structure of Sr<sub>2</sub>P<sub>2</sub>O<sub>7</sub> but caused only small shifts in the XRD patterns of doped samples. In those studies, it was pointed out that the thermoluminescence glow curve of pure Sr<sub>2</sub>P<sub>2</sub>O<sub>7</sub> includes only one glow peak at around 100 °C. On the other hand, Pr along Cu-doped samples resulted with very intense, sharp peaks in TL glow curves around 200°C. For this reason, the TL properties of this material were studied in detail in the given present study.

The results in this study indicated that the reproducibility of integrated areas of glow peaks of Cu and Pr-doped Sr<sub>2</sub>P<sub>2</sub>O<sub>7</sub> highly depend on the annealing temperature, time and preceding dose level applied to the dosimeter before usage. The additive dose method indicated that the peak temperatures of the glow peaks do not shift towards lower and/or higher temperature sides with increasing dose levels. The similar results were also obtained for T<sub>1</sub> and T<sub>2</sub> of both glow peaks. Therefore, their geometric shape factors ( $\mu_g$ ) were not changed with increasing dose levels. These results show that both of the glow curves should have first-order glow peaks. On the other hand, the  $T_m-T_{stop}$  procedure shows that the position of dosimetric peak shifts towards the high temperature side with increasing stopping temperature. This result meant that the dosimetric peak of studied material can be best described with general-order kinetics. A detail analysis of this peak with other methods such as additive dose, peak shape,  $E_a-T_{stop}$ , and CGCD methods indicated that this peak have general-order kinetics. The similar result was also obtained for first peak. But, it was observed that its order is always close to first-order kinetic. The results of  $T_m-T_{stop}$  and additive dose experiments were also indicated that the kinetic parameters of these peaks determined by peak shape, initial rise and CGCD methods are dependent

on the experimental parameters such as dose level and heat treatment after the irradiation. These results determine that there is no good consensus or agreement between the results obtained by various techniques. Actually, the results of variable heating rate methods are very different than the others. Additionally, the determined activation energy values found by IR, CGCD and PS methods for the dosimetric peak approach to each other and they reach  $1.3 \pm 0.1$  eV which is highly different result obtained by VHR method. One possible explanation for the confliction on the value of kinetic parameters is that the variation in the emission spectrum with temperature, self-absorption, thermal quenching and application of a high heating rate are some possibilities for causing distortions in the glow curve shape which in turn have an effect on the evaluated kinetic parameters of Cu and Pr-doped  $\text{Sr}_2\text{P}_2\text{O}_7$  samples. Moreover, a distribution of activation energies and frequency factors may cause a variation of the estimated kinetic parameters. On the other hand, some of the important dosimetric properties of this material such as its TL sensitivity, dose response and simple TL glow curve shapes were suggesting that this material could use as a dosimetric material in the radiation dose measurements.

## References

- [1] A. N. Yazici, H. Toktamis, S. Seyyidoglu, A. Yilmaz. (2010). Thermoluminescent properties of  $\text{Sr}_2\text{P}_2\text{O}_7$  doped with copper and some rare earth elements, *Journal of Luminescence*, **130**, 1744–1749.
- [2] S.W.S. McKeever. (1985). Thermoluminescence of Solids, *Cambridge University Press*, Cambridge.
- [3] C. Furetta, S.Guzman, B.Ruiz, E.Cruz-Zaragoza. (2011). *Applied Radiation and Isotopes*, **69**, 346–349 Available at: [www.elsevier.com](http://www.elsevier.com) Accessed 17.01.2011.
- [4] Sangmoon Park, Thomas Vogt. (2009). Luminescent phosphors, based on rare earth substituted oxyfluorides in the  $\text{A}(1)_{3-x}\text{A}(2)_x\text{MO}_4\text{F}$  family with  $\text{A}(1)/\text{A}(2)=\text{Sr, Ca, Ba}$  and  $\text{M}=\text{Al, Ga}$ , *Journal of Luminescence* **129**, 952-957.
- [5] Victoria V.Chernaya, Alexander S. Mitiaev, Pavel S. Chizhov, Evgeny V. Dikarev, Roman V. Shpanchenko, Evgeny V. Antipov, Mikhail V. Korolenko, and Pavel B. Fabritchnyi A.S.Mitaev, P.S.Chizhov, E.V.Dikarev, R.V.Shpanchenko. (2005). Synthesis and Investigation of Tin(II) Pyrophosphate  $\text{Sn}_2\text{P}_2\text{O}_7$ , *Chemistry of Materials*, **17**,284-290.
- [6] M.Ferid, K.Horchani, J.Amami, Mokhtar Ferid, Karima Horchani, Jaouher Amami. (2004). Preparation, structure and infrared spectrum of  $\text{NaEuP}_2\text{O}_7$ , *Materials Research Bulletin*, **39**,1949-1955.
- [7] K. Horchani-Naifer, J. Amami, M. Férid. (2009). Synthesis and crystal structure of sodium praseodymium polyphosphate,  $\text{NaPr}(\text{PO}_3)_4$ , *Journal of Rare Earths*, **27**, 1-3.
- [8] Halil Guler and Figen Kurtulus. (2005). A microwave-assisted route for the solid-state synthesis of lead pyrophosphate,  $\text{Pb}_2\text{P}_2\text{O}_7$ , *Journal of Materials Science* **40**, 6565-6569.
- [9] R.K.B Gover, N.D. Withers, S. Allen, R.L. Withers, J.S.O. Evans. (2002). Structure and Phase Transitions of  $\text{SnP}_2\text{O}_7$ , *Journal of Solid State Chemistry*, **166**, 42-48.
- [10] R.L. Withers, Y. Tabira, J.S.O. Evans, I.J. King, A.W. Sleight. (2001). A New Three-Dimensional Incommensurately Modulated Cubic Phase (in  $\text{ZrP}_2\text{O}_7$ ) and Its Symmetry Characterization via Temperature-Dependent Electron Diffraction, *Journal of Solid State Chemistry*, **157**, 186-192.
- [11] N. Khay, A. Ennaciri. (2001). Vibrational spectra of double diphosphates  $\text{CsLnP}_2\text{O}_7$  ( $\text{Ln}=\text{Gd, Tb, Dy, Ho, Y, Er, Tm, Yb}$ ), *Journal of Alloys and Compounds*, **323–324**, 800-805.

- [12] N. Khay, A. Ennaciri, M. Harcharras. (2001). Vibrational spectra of double diphosphates  $\text{RbLnP}_2\text{O}_7$  ( $\text{Ln} = \text{Dy}, \text{Ho}, \text{Y}, \text{Er}, \text{Tm}, \text{Yb}$ ), *Vibrational Spectroscopy*, **27**, 119-126.
- [13] V.V Lisnyak, N.V Stus, N.S Slobodyanik, N.M Belyavina, V.Ya Markiv. (2000). Crystal structure of a novel cubic pyrophosphate  $\text{WP}_2\text{O}_7$ , *Journal of Alloys and Compounds*, **309**, 83-87.
- [14] Shao-Long Tie, Yuan-Ying Li, Yan-Sheng Yang. (1997). Structure and vibration spectra of new pseudo-pyrophosphate  $\text{NaDyP}_2\text{O}_7$ , *Journal of Physics and Chemistry of Solids*, **58**, 957-959.
- [15] Ioan-Cezar Marcu, Jean-Marc M. Millet and Jean-Marie Herrmann. (2001). Semiconductive and Redox Properties of Ti and Zr Pyrophosphate Catalysts ( $\text{TiP}_2\text{O}_7$  and  $\text{ZrP}_2\text{O}_7$ ). Consequences for the Oxidative Dehydrogenation of n-Butane, *Catalysis Letters*, **78**, 273-279.
- [16] C.H. Kim, H.S. Yim. (1999). The effect of tetravalent metal on dielectric property in  $\text{ZrP}_2\text{O}_7$  and  $\text{TiP}_2\text{O}_7$ , *Solid State Communications*, **110**, 137-142.
- [17] Koji Amezawa, Yukinori Kitajima, Yoichi Tomii, Naoichi Yamamoto, Marius Widere. (2005). Truls Norby Protonic conduction in acceptor-doped  $\text{LaP}_3\text{O}_9$ , *Solid State Ionics*, **176**, 2867-2870.
- [18] A. Doat, F. Pellé. (2005). A. Lebugle, Europium-doped calcium pyrophosphates: Allotropic forms and photoluminescent properties, *Journal of Solid State Chemistry*, **178**, 2354-2362.
- [19] W.J Schipper, J.J Piet, H.J De Jager, G Blasse. (1994). On the luminescence of hafnium compounds, *Materials Research Bulletin*, **29**, 23-30.
- [20] Hassane Assaaoudi, Ian S. Butler, Janusz A. Kozinski. (2006). Crystal structure and vibrational and luminescence spectra of a new erbium potassium pyrophosphate dihydrate,  $\text{ErKP}_2\text{O}_7 \cdot 2\text{H}_2\text{O}$ , *Solid State Sciences*, **8**, 1353-1360.
- [21] Li, M.-R., Liu, W., Chen, H.-H., Yang, X.-X., Wei, Z.-B., Cao, D.-H., Gu, M. and Zhao. (2005). Low-Temperature Flux Synthesis, Crystal Structure and Ce-Doped Luminescence of the First Lutetium Diphosphate  $\text{NH}_4\text{LuP}_2\text{O}_7$ . *European Journal of Inorganic Chemistry*, **2005**, 4693-4696.
- [22] A.Necmeddin Yazici, Mustafa Öztaş, V.Emir Kafadar, Metin Bedir, Hüseyin Toktamış. (2007). The analysis of thermoluminescent glow peaks of copper doped ZnS thin films after  $\beta$ -irradiation *Journal of Luminescence*, **124**, 58-66.
- [23] K. Zen Keizars, Beth M. Forrest, and W. Jack Rink. (2008). Thermoluminescence as a Method of Analysis of Sand Transport along the Coast of the St. Joseph Peninsula, Florida, *Journal of Coastal Research*. **24**, 500-507

- [24] Krystyna Palewska, Andrzej Miniewicz, Stanislaw Bartkiewicz, Janina Legendziewicz, Wieslaw Strek. (2007). Influence of electric field on photoluminescence of lanthanide-doped nematic liquid crystal, *Journal of Luminescence*, **124**, 265-272.
- [25] V. Natarajan, M.K. Bhide, A.R. Dhobale, S.V. Godbole, T.K. Seshagiri, A.G. Page, Chung-Hsin Lu. (2004). Photoluminescence, thermally stimulated luminescence and electron paramagnetic resonance of europium-ion doped strontium pyrophosphate, *Materials Research Bulletin*, **39**, 2070-2075.
- [26] Srivastava A.M. (2003). *US patent application*, **003**,006,7008.
- [27] M. Férid, K. Horchani-Naifer. (2004). Synthesis, crystal structure and vibrational spectra of a new form of diphosphate  $\text{NaLaP}_2\text{O}_7$ , *Materials Research Bulletin*, **39**, 2209-2217.
- [28] J. Belkouch, L. Monceaux, E. Bordes, P. Courtine. (1995). Comparative structural study of mixed metals pyrophosphates, *Materials Research Bulletin*, **30**, 149-160.
- [29] Aliou Hamady, Mohamed Faouzi Zid, Tahar Jouini. (1994). Structure Cristalline de  $\text{KYP}_2\text{O}_7$ , *Journal of Solid State Chemistry*, **113**, 120-124.
- [30] Shumin Wang, Shiou-Jyh Hwu. (1991). Brief communication Completion of the alkali metal titanium (III) pyrophosphate series: Synthesis and structure of, *Journal of Solid State Chemistry*, **92**, 219-226.
- [31] V.Trunov, Y.V. Oboznenko, S.P. Sirotkin, N.B. Tskheasvili. (1991). *Inorganic materials*, **27**, 2026-2029.
- [32] S. Ledain, A. Leclaire, M. M. Borel and B. Raveau. (1996). inorganic compounds  $\text{LiMoP}_2\text{O}_7$ , *Acta Crystallographica Section C*, **52**, 1593-1594.
- [33] A. Bouffessi, A. Boukhari, E.M. Holt. (1996). inorganic compounds  $\text{LiMoP}_2\text{O}_7$ , *Acta Crystallographica Section C*, **52**, 1594-1599.
- [34] Rui Fontes, Diogo Fernandes, Filipe Peralta, Hugo Fraga, Inês Maio, Joaquim C. Esteves da Silva.(2008). Pyrophosphate and tripolyphosphate affect firefly luciferase luminescence because they act as substrates and not as allosteric effectors, *FEBS Journal*, **275**, 1500-1509.
- [35] S. Idrissi, M. Rghioui, L. Nejjar, R. Benarafa, L. Saidi Idrissi, M. Lorriaux, A. Wallart. (2004). Molecular and Biomolecular Spectroscopy, *Spectrochimica Acta, Part A*, **60**, 2043-2052.
- [36] N. Stock, G. Ferey, A.K. Cheetham. (2000). Hydrothermal synthesis and characterization of a chromium(II) pyrophosphate,  $\text{Na}_2\text{CrP}_2\text{O}_7 \cdot 0.5\text{H}_2\text{O}$  *Solid State Sciences*, **2**, 307-312.

- [37] H. Assaaoudi, I. Butler, J. Kozinski, F. Belanger-Gariepy. (2005). *Journal of Chemical Crystallography*, 35, 809-820.
- [38] T. Varga, A. Wilkinson, M. Haluska, E. Payzant. (2005). Preparation and thermal expansion of  $(M^{III}_{0.5} M^V_{0.5})P_2O_7$  with the cubic  $ZrP_2O_7$  structure *Journal of Solid State Chemistry*, 178, 3541-3546.
- [39] H. Miyoshi, T. Yoshino. (1996). *Radiation Physics and Chemistry*, 48, 315-318.
- [40] H. Kundua, P. Massnda, P. Marathe, G.Venkatamarana. (1980). *Nuclear Instruments and Methods*, 15, 363-367.
- [41] Semih Seyyidođlu, Macit Özenbař, Necmeddin Yazıcı and Ayřen Yılmaz. (2007). Investigation of solid solution of  $ZrP_2O_7-Sr_2P_2O_7$ , *Journal of Materials Science*, 42, 6453-6463.
- [42] DOĐAN Mehmet. (2007). Development of New Sensitive Thermoluminescent Materials for Radiation Dosimetry, *Gaziantep Üniversitesi, Fen Bilimleri Enstitüsü*.
- [43] Aitken M.J. (1985). Thermoluminescence Dating, Academic Press, London.
- [44] McKeever, S.W.S., Moscovitch, M. and Townsend, P.D. (1995). Thermoluminescence Dosimetry Materials: Properties and Uses, Nuclear Technology Publishing, Kent.
- [45] Farrington Daniels, Charles A. Boyd, and Donald F. Saunders. (1953). Thermoluminescence as research tool, *Science*, 117, 343.
- [46] Kortov V. (2007). Materials for thermoluminescent dosimetry: Current status and future trends, *Radiation Measurements*, 42, 576-581.
- [47] Y.S. Horowitz, D. Yossian. (1995). Computerised glow curve deconvolution: application to thermoluminescence dosimetry Monograph, *Radiation, Protection Dosimetry*, 60, 1.

- [48] K. Mahesh, P.S. Weng, C. Furetta, (1989), *Thermoluminescence in Solids and its Applications*, Nuclear Technology Publishing, Ashford.
- [49] R. Chen, S.W.S. McKeever. (1997). Theory of Thermoluminescence and Related Phenomena, World Scientific Publications, London, NJ, Singapore, 576.
- [50] R. Chen, Y. Kirsh. (1981). Analysis of Thermally Stimulated Processes, Pergamon, Oxford.
- [51] Azorin J., Furetta C. and Gutierrez A. (1993). preparation and properties of thermoluminescent materials, *Physics Solid State*, **138**, 9-46.
- [52] Meyer G. (1982). The synthesis and structures of complex rare-earth halides *Progress in Solid State Chemistry*, **14**, 141.
- [53] Vij, D.R., Editor. (1993). Thermoluminescent Materials, PTR Prentice-Hall, New Jersey.
- [54] Y.S. Horowitz and D. Yossian. (1995). Computerized Glow Curve Deconvolution: Application to Thermoluminescence Dosimetry, *Radiation Protection Dosimetry*, **60**, 1-114.
- [55] C. Furetto, Pao-Shan Weng. (1998). Operational Thermoluminescence Dosimetry, World Scientific, Singapore.
- [56] A.N.Yazıcı. (1996). Thermal and optical Characteristics of Radiation Induced Defect Centers in Alkali Halide Crystal, PhD Thesis, Gaziantep University.
- [57] V.E.Kafadar, A.Necmeddin Yazıcı and R.Güler Yıldırım. (2009). Determination of trapping parameters of dosimetric thermoluminescent glow peak of lithium triborate (LiB<sub>3</sub>O<sub>5</sub>) activated by aluminum” *Journal of Luminescence*, **129**, 710-714.
- [58] J.T. Randall and M.H.F. Wilkins. (1945). Phosphorescence and. Electron Traps: I Study of Trap Distributions, *Proc. R. Soc. London Ser.A*, **184**, 366.
- [59] J.T. Randall and M.H.F. Wilkins. (1945). Phosphorescence and Electron Traps: II The Interpretation of Long-Period Phosphorescence, *Proc. R. Soc. London Ser. A*, **184**, 390.
- [60] A.J.J. Bos. (2001). High sensitivity thermoluminescence dosimetry, Nuclear Instruments & methods in Physics Research Section B: Beam Interactions with Materials and Atoms, **184**, 3-28.
- [61] C.Furetta. (2003). Handbook of Thermoluminescence, World Scientific Publishing.

- [62] G. Kitis, J.M. Gomez-Ros and J.W.N. Tuyn. (1998). Thermoluminescence glow- curve deconvolution functions for first, second and general orders of kinetics, *Journal of Physics D:Applied Physics*, **31**, 2636-2641.
- [63] A.J.J.Bos, T.M.Piters, J.M.Gómez Ros, and A.Delgado. (1993). GLOCANIN, an Intercomparison of Glow Curve Analysis Computer Programs, *IRI-CIEMAT Report* **131**-93-005.
- [64] G.F.J. Garlick and A.F.Gibson. (1948). The electron trap mechanism of luminescence in sulphide and silicate phosphors, *Proceedings of the Physical Society*, **60**, 574-590.
- [65] A.J.J. Bos and J.B. Dielhof. (1991). The Analysis of Thermoluminescent Glow Peaks in CaF<sub>2</sub>:Tm (TLD-300), *Radiation Prot. Dosim.*, **36**, 231.
- [66] C.E. May and J.A. Partridge. (1964). Thermoluminescent kinetics of alpha irradiated alkali halides, *Journal of Chemical Physics*, **40**, 1401-1409.
- [67] R. Chen and A.A. Winer. (1970). Effects of various heating rates on glow-curves, *Journal of Applied Physics*, **41**, 5227.
- [68] R. Chen. (1969). On the Calculation of the Activation Energies and Frequency Factors from Glow- Curves, *Journal of Applied Physics*, **40**, 570.
- [69] L. I. Grossweiner. (1953). A note on the analysis of first-order glow curves, *Journal of Applied Physics*, **24**, 1306.
- [70] A. Halperin and A.A Braner. (1960). Evaluation of Thermal Activation Energies from Glow Curves, *Physics Rev*, **117**, 405.
- [71] S. P. Kathuria and C. M. Sunta. (1979). Kinetics and trapping parameters of thermoluminescence in LiF TLD-100-dependence on dose, *Journal of Physics D: Applied Physics*, **12**, 1573.
- [72] N. S. Mohan and R. Chen. (1970). Numerical Curve Fitting for calculating Glow Parameters, *Journal of Physics D: Applied Physics*, **3**, 243-247.
- [73] D. Shenker and R. Chen. (1972). Numerical Solution of the Glow Curve Differential Equations, *Journal Comp. Physics*, **10**, 272-283.
- [74] H.G. Balian and N.W. Eddy. (1977). Figure-of-Merit (FOM), an Improved Criterion over the Normalized Chi-Squared Test for Assessing Goodness-of-Fit of Gamma-Ray Spectra Peaks, *Nuclear Instrumentation Methods*, **145**, 389-395.
- [75] S. K. Misra and N.W.Eddy. (1979). IFOM, a Formula for Universal Assessment of Goodness-of- Fit of Gamma Ray Spectra, *Nuclear Instrumentation Methods*, **166**, 537-540.



- [76] A.Necmeddin Yazıcı and M.Yakup Hacıbrahimoglu and Metin Bedir. (2001). Determination of the Trapping Parameters of Glow Peaks of  $\text{CaF}_2$ :Dy (TLD-200) by Using Computer Glow Curve Deconvolution Method, *Turk Journal of Physics*, **25**, 249-255.
- [77] Kitis G. and Pagonis V. (2007). Peak shape methods for general-order thermoluminescent glow peaks: a reappraisal, *Nuclear Instrumentation Methods B*, **262**, 313-322.
- [78] Altermatt UD, Brown ID. (1987). Bond-valence parameters obtained from a systematic analysis of the Inorganic Crystal Structure Database, *Structural Science*, **41**, 244-247.
- [79] Tolga Depci, Gülhan Özbayoğlu, Ayşen Yılmaz, A. Necmeddin Yazıcı. (2008). The thermoluminescent properties of lithium triborate ( $\text{LiB}_3\text{O}_5$ ) activated by aluminium, *Nuclear Instruments and Methods in Physics Research Section B: Beam Interactions with Materials and Atoms*, **266** 755-762.
- [80] C. Christodoulides. (1985). Errors involved in the determination of activation energies in TL and TSDC by the initial rise method, *Journal of Physics D: Applied Physics*, **18**, 1665.
- [81] T.S.C. Singh, P.S. Mazumdar, R.K. Gartia. (1988). On the determination of activation energy in thermoluminescence by the initial rise method, *Journal of Physics D: Applied Physics*, **21**, 1312.
- [82] A. Necmeddin Yazici, Solak Semra, Öztürk Zihni, Tokasu Mustafa, Yegingil Zehra. (2003). The analysis of dosimetric glow peak of  $\alpha$ - $\text{Al}_2\text{O}_3$ :C after different dose levels by  $\beta$ - irradiation, *Journal of Physics D: Applied Physics* **36**, 181.
- [83] A Necmeddin Yazici and Mustafa Topaksu. (2003). *The analysis of thermoluminescence glow peaks of unannealed synthetic quartz* Journal of Physics D: Applied Physics. **36**, 620.
- [84] A.S. Pradhan. (2002). Effect of heating rate on the responses of  $\text{CaF}_2$ :Cu,  $\text{CaF}_2$ :Tm,  $\text{CaF}_2$ :Dy and  $\text{CaF}_2$ :Mn, *Radiat. Prot. Dosim.* **100**, 289.
- [85] S.G. Gorbics, A.E. Nash, F.H. Attix. (1969). Thermal quenching of luminescence in six thermoluminescent dosimetry phosphors – II:quenching of thermoluminescence, *Inter. Journal Applied. Radiation. Isotopes*, **20**, 843.
- [86] A.J.J. Bos, T.M. Pitters, J.M. Gómez-Ros, A. Delgado. (1993). An intercomparison of glow curve analysis computer programs: I. Synthetic glow curves, *Radiation. Protection Dosimeter*, **47**, 473.